HAL
open science

THE PHYSICS OF THE EARTH'S COLLISIONLESS SHOCK WAVE

V. Formisano

To cite this version:

V. Formisano. THE PHYSICS OF THE EARTH'S COLLISIONLESS SHOCK WAVE. Journal de Physique Colloques, 1977, 38 (C6), pp.C6-65-C6-88. 10.1051/jphyscol:1977608 . jpa-00217192

HAL Id: jpa-00217192

https://hal.science/jpa-00217192

Submitted on 4 Feb 2008

HAL is a multi-disciplinary open access archive for the deposit and dissemination of scientific research documents, whether they are published or not. The documents may come from teaching and research institutions in France or abroad, or from public or private research centers.

L'archive ouverte pluridisciplinaire **HAL**, est destinée au dépôt et à la diffusion de documents scientifiques de niveau recherche, publiés ou non, émanant des établissements d'enseignement et de recherche français ou étrangers, des laboratoires publics ou privés.

THE PHYSICS OF THE EARTH'S COLLISIONLESS SHOCK WAVE

V. FORMISANO (*)

Laboratorio Plasma Spazio, CNR-Frascati, Italy

Résumé. — Un choc d'étrave sans collision formé d'un mode rapide, est un phénomène permanent de l'interaction du vent solaire avec la terre. Le choc est approximativement stationnaire dans les coordonnées de la terre ; sa structure, cependant, change avec la position en raison des différentes valeurs de $\mathbf{B}.\mathbf{n}$, et avec le temps en raison des différentes conditions du vent solaire (nombre de Mach M et β, T_e/T_i...). Le choc d'étrave de la terre se révèle comme un outil impressionnant d'étude des ondes de choc sans collision. Après les efforts théoriques importants dans l'étude des ondes de choc dans le passé, il est possible, aujourd'hui, de vérifier expérimentalement que différents mécanismes de dissipation interviennent dans différents régimes du plasma. L'examen extensif de la morphologie du choc d'étrave nous permet aujourd'hui, de corréler les caractéristiques de la structure du choc d'étrave, que révèlent une variété de diagnostics, avec M, β et Bn dans le vent solaire. Pour des géométries quasi parallèles, et apparemment pour n'importe quels M et β, la couche du choc s'élargit et se casse, en présentant un niveau limité de bruit d'ondes de plasma et des effets marqués de précurseur. Pour des ondes de choc quasi perpendiculaires, au contraire, la turbulence électromagnétique augmente avec β, presqu'indépendamment de M ; alors que le niveau de bruit électrostatique augmente avec M, presqu'indépendamment de β. La comparaison avec les différentes théories valables pour les différents régimes de plasma est la tâche ici entreprise.

Abstract. — A fast mode collisionless bow shock is a permanent feature of the solar wind interaction with the earth. The shock is approximately stationary in earth coordinates, its structure, however, changes in space due to different $\widehat{\mathbf{Bn}}$ values, and in time, due to different solar wind conditions (Mach number M and β, T_e/T_i...). The earth's bow shock has revealed itself as an impressive tool for studying collisionless shock waves. After the large theoretical efforts in studying collisionless shock waves, in the past, it is possible, today, to verify experimentally that different dissipation mechanisms are at work in different plasma regimes. The extensive examination of bow shock morphology allow us, today, to correlate distinctions in bow shock structure, revealed by a variety of diagnostics, with M, β and Bn in the solar wind. For quasi parallel geometries and apparently for any M and β, the shock layer broadens and breacks up, showing limited level of plasma wave noise and marked precursor effects. For quasi perpendicular shock waves, on the contrary, electromagnetic turbulence increases with β, almost independent of M ; while electrostatic noise level increase with M, almost independent of β. Comparison with the different theories valid in the different plasma regimes is the present task.

1. **Introduction.** — The solar wind is a tenuous plasma with a frozen-in magnetic field, flowing always radially out of the solar corona. This plasma has almost constantly three components : electrons, protons and alpha particles. Occasionally other heavier ions may be present. The average values of the solar wind parameters are : proton density $N_p \simeq 5$ p/cm^3, bulk speed $V_p \simeq 400$ km/s, temperature $T_p \simeq 7 \times 10^4$ K ; electron density $N_e \simeq N_p$, bulk speed $V_e \simeq V_p$ and temperature $T_e \simeq 1.5 \times 10^5$ K ; α-particle density $N_\alpha \simeq 0.05\, N_p$ bulk speed $V_\alpha \simeq V_p$ and $T_\alpha \simeq 4\, T_p$ (see reference [1] and references therein).

(*) Present address : Space Science Department of ESA, European Space Research and Technology Centre, Noordwijk, The Netherlands.

These values characterize the interplanetary space plasma as being very different from the Laboratory plasmas, and certainly as being collisionless (in terms of classical Coulombian collisions).

In its expansion away from the solar corona, the solar wind interacts with all the planetary objects, in particular with the earth's magnetospheric cavity. The result of this interaction is a collisionless shock wave standing almost 2-5 R_E away from the surface delimiting the magnetospheric cavity (see Fig. 1).

Most of the artificial satellites of the earth have had an apogee large enough ($>$ 15-20 R_E) to encounter every orbit twice the bow shock wave, a relevant number of more or less complete observations of the shock structure have, therefore, been provided, causing a deep interest of space physicists in collisionless shock waves.

Article published online by EDP Sciences and available at http://dx.doi.org/10.1051/jphyscol:1977608

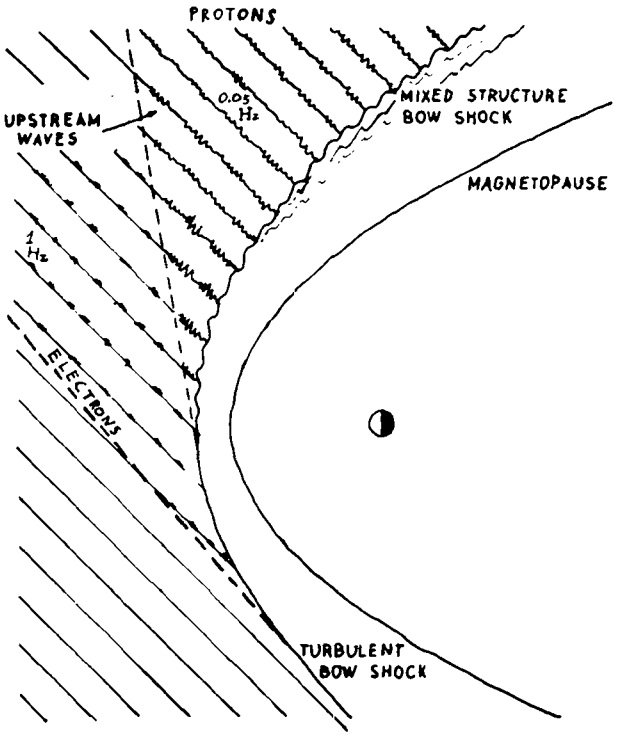

FIG. 1. — Schematic sketch in the ecliptic plane of the interaction between the solar wind and the Earth's magnetic field. The magnetopause and the bow shock are indicated together with the region where the particles reflected at the bow shock interact with the incoming plasma generating four kinds of wave phenomena (Sect. 8) [4].

The study of the earth's bow shock has revealed itself to be a much more profitable tool than laboratory collisionless shock experiments mainly because of the high variability of the upstream plasma conditions.

Indeed, while in the laboratory plasma the upstream conditions were roughly constant or varied within defined short ranges of values, the solar wind plasma parameters may change more than a factor 100 if a large enough time interval (a few months) is considered. All the plasma parameters which are important for the physics of a collisionless shock wave are expected to vary, in the case of the earth's bow shock, over ranges so vast to reveal the different possible shock structures : for example values of β (ratio of particles internal pressure divided by magnetic pressure) as low as 0.01 and as large as 100 have been observed ; the solar wind Alfvénic mach number has been observed to change between ~ 1.2 and $\simeq 20$; given a magnetic field direction upstream, also the value of $\widehat{\mathbf{Bn}}$ (angle between magnetic field direction and shock normal) changes from $\simeq 0^\circ$ to 90° in different locations of the geometry. The highly varying upstream conditions if allowed the study of the shock in many different plasma regimes, causes two important difficulties : the shock, in most cases, cannot be considered as being stationary, but moves with respect to the satellite, with an unknown velocity. Also this satellite-shock relative speed has been shown experimentally to vary from $\lesssim 1$ km/s to $\gtrsim 100$ km/s, but in most cases the shock speed is unknown, and therefore it is not possible to quote absolute values of the dimensions involved in the observations. This problem will be solved with the ISEE-A and B missions (to be launched late in 1977), when a pair of satellites travelling at a known, small distance from one to the other, will allow the separation of space versus time variations.

Another difficulty caused by the highly variable value of solar wind parameters, is the fact that the shock wave has, in the data collected by the satellites, an aspect that seems to be continually different and never repeated. This fact has brought some authors to the conclusion that the earth's collisionless shock wave is unstable. Today this difficulty has been solved by collecting and studying shock observations referring to the same upstream parameter values.

In this review we have mostly ignored experimental results obtained in Laboratory plasma physics experiments, although we are aware of the importance of the results present in the literature. The reader is referred to [2-6] for a discussion of Laboratory experiment results.

2. **Classification of shock structures.** — A priori the collisionless shock properties can be different for different upstream conditions, for example it is clear that a parallel shock, $\widehat{Bn} \simeq 0^\circ$, will be different from a perpendicular shock, $\widehat{Bn} \simeq 90^\circ$.

There is, therefore, a need for a classification of shock structures. But which should be the criterion ? Certainly $\widehat{Bn}$ should be one of the most important parameters to be considered.

In reference [7] Sagdeev classified the shock structures on the basis of the role of the turbulence present in the shock layer : It is necessary for this turbulence to have dissipation, and therefore an increase of entropy, otherways theoretically only solitons or infinite wave trains are found. On the basis of the role of the shock turbulence, theoretically, laminar shocks, turbulent shocks and mixed structures have been distinguished [8]. Laminar shocks are those in which the microturbulence is present only in the shock ramp and has small amplitude. Quantitatively laminar shocks are those in which the quantity

$$C = -\frac{e}{m}\left\langle \delta\bar{E} + \frac{1}{c}\bar{v}x\,\delta\bar{B}\right\rangle \cdot \frac{\partial\delta f}{\partial\bar{v}} \qquad (1)$$

is $\neq 0$ but small. In eq. (1) the δ indicates the fluctuating part of the following quantity, and $< \; >$ indicates the ensemble average ; f is the particles distribution function. The quantity C plays the role in the shock equations, of a collision term as it is the quantity that may change the average value of the other quantities. Turbulent shocks are those with $C \neq 0$ and large ; mixed structures are those in

which the laminar profile is partially destroyed by transfer of energy from the principal laminar oscillation to plasma fluctuations through mode coupling. This classification does not specify the nature of the turbulence present in the shock.

When dealing with actual shocks, the nature of the turbulence, however, has to be specified in order to identify the upstream parameters that should be considered. It is well known that many different theories have been developed for collisionless shock waves, each one introducing a different turbulence in the structure, we find therefore many parameters in the literature that are said to be important for the shock structure. Let us list here some of them :

$\widehat{\mathbf{Bn}}$: angle between the magnetic field direction and the shock normal

$\widehat{\mathbf{Vn}}$: angle between the plasma bulk velocity and the shock normal.

$$M_A = V/\{ B/(4\,\pi n m_i)^{1/2} \} \quad \text{Alfvénic Mach number.}$$

$$M_F = V/\{ B^2/(4\,\pi n m_i) + k(n m_i\, T_i + n m_e\, T_e) \}^{1/2} \quad \text{Fast Mach number.}$$

$$\beta = \frac{2\,\pi k(n m_i\, T_i + n m_e\, T_e)}{B^2} \text{ : The ratio of thermal to magnetic pressure.}$$

$$\alpha = \Omega_e/\omega_{pe} = \left(\frac{B^2\,\varepsilon_0}{c^2\, m_e\, n_e}\right) \text{ : The ratio of electron-gyro to plasma frequency.}$$

T_e/T_i : The ratio of electron to ion temperature.
N_p/N_{imp} : The ratio of the density of the principal ion compound to the secondary ion compound.

The importance of some of these parameters changes from one theory to another, depending on the turbulence implied by the dissipation mechanism. For some of them, however, a well defined role has been established. $\widehat{\mathbf{Bn}}$, for example, defines the obliquity of the shock : if $\cos \widehat{\mathbf{Bn}} < \sqrt{m_e/m_i}$ the shock is perpendicular, if $\widehat{\mathbf{Bn}} \lesssim 10^{\circ}$ the shock is parallel, in between the shock is oblique. The Mach number certainly is another important parameter : for low Mach numbers the shock should be dispersive (resistive), above a value M^* (called critical Mach number) the resistivity in the shock layer is not enough to explain the larger dissipation of ordered energy, therefore viscosity has to be introduced ; at still larger Mach numbers M^{**}, wave breaking occurs therefore forbidding laminar structures. The critical Mach number, on the other hand, is a function of $\widehat{Bn}$ and β (Figs. 2*a*, *b*) [9, 10]. The critical Mach number has been introduced mainly for the Alfvénic Mach number ; the earth's bow shock is, however, a fast shock, so the relevant Mach number is the fast Mach number, and for high values of β, M^* falls asymptotically to 1, meaning that at very high β

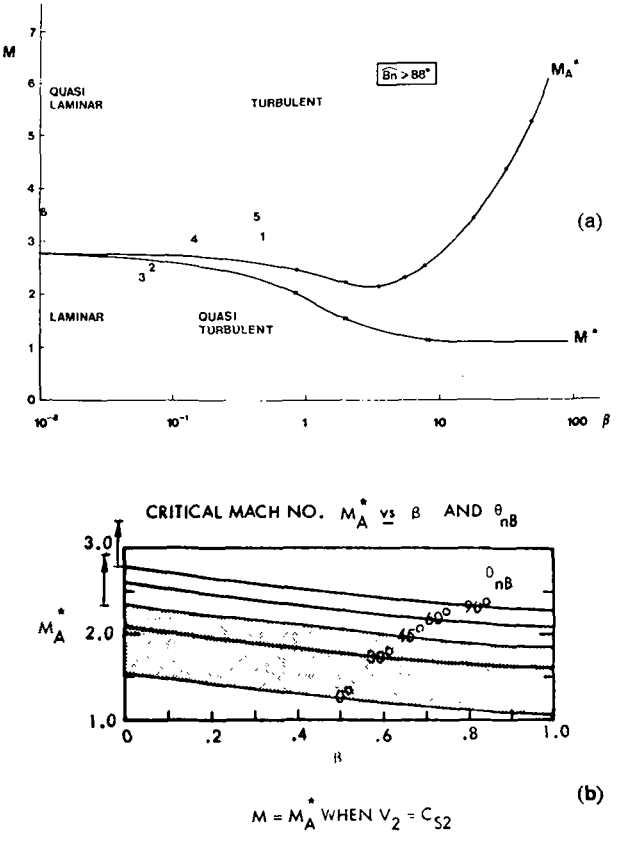

FIG. 2. — Dependence of the critical Mach number (Alfvenic M_A or magnetosomic M) on β for perpendicular (*a*) or oblique (*b*) shock structures [24].

resistive shocks cannot exist. Some of the listed parameters may be important only in particular cases : T_e/T_i is of relevance only if electrostatic ion-acoustic noise is present in the shock layer ; N_{imp}/N_p is important only if a relevant percentage of a second species of ions is present : in this case, indeed, it has been shown that small concentrations of ions of a second species can drastically alter the structure of the shock and the potential drop φ_m across it [11].

Experimentally the importance of β, M, $\widehat{\mathbf{Bn}}$ and T_e/T_i has been verified.

The very low frequency magnetic fluctuations observed downstream of the bow shock, indeed, have an amplitude decreasing with increasing value of $\widehat{Bn}$ (perpendicular shocks are less turbulent ; see figure 3). Reducing the data to the same value of $\widehat{Bn}$ (= 45°) the amplitude of the magnetic fluctuations increases with increasing values of β (Fig. 4). We shall see in section 6 that higher frequency electromagnetic noise has a different behaviour.

The electrostatic noise, on the other hand, has been shown in reference [12] (see also Ref. [13]) to have an amplitude increasing with an increasing value of T_e/T_i (Fig. 5), although the data points appear to be scattered over rather large ranges of values. This

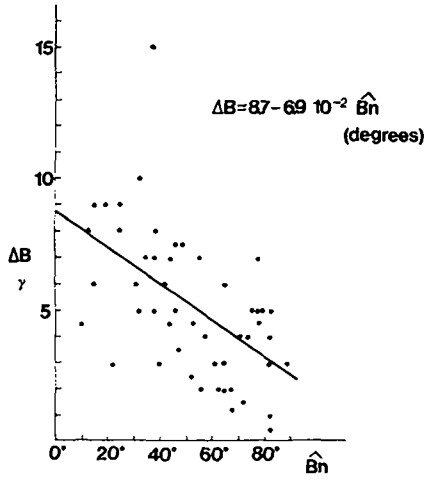

FIG. 3. — Relationship between the amplitude of the very low frequency magnetic noise observed in the first 20 min. downstream of the bow shock and upstream $\widehat{Bn}$. The line gives the best fit to the points [23].

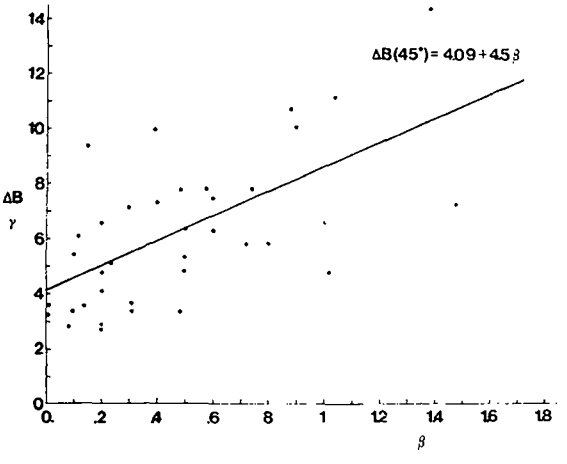

FIG. 4. — Relationship between the amplitude of the very low frequence magnetic noise observed in the first 20 min. downstream of the bow shock and upstream β. The line gives the best fit to the points obtained after normalizing the actual measurements to the same $\widehat{Bn}$ (= 45°) through the relationship found in figure 3 [23].

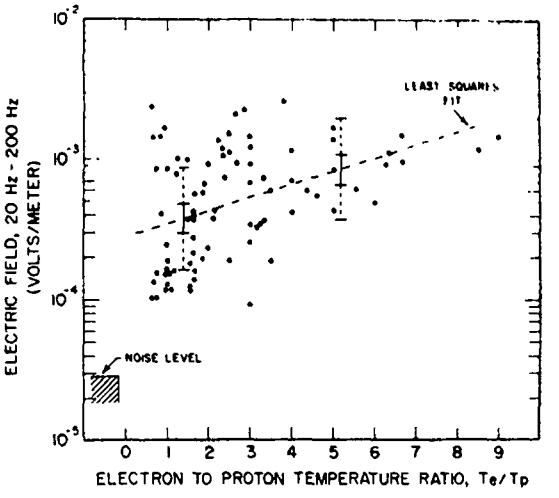

FIG. 5*a*. — Plot of $E'_{\mathrm{rms},2}$, the rms field strength of the electrostatic component of the shock spectrum (200 Hz to 4 kHz), against T_e/T_p showing a strong positive correlation. The dashed diagonal line is the line of regression for a least squares fit to the equation $\log y = bx + a$, where $y = E_{\mathrm{rms},2}$ and $x = T_e/T_p$. The slope of the regression line, which is the important measure of association, has a dispersion which is indicated by rotating the regression line about its centroid to the limits indicated by the small error bars at $\pm$ 2.576 $\sigma(y)$. The large error bars at $\pm$ $\sigma(y)$ probably arise from short-period fluctuations in T_e/T_p and from correlations with other upstream parameters not considered in this two-parameter fit [12].

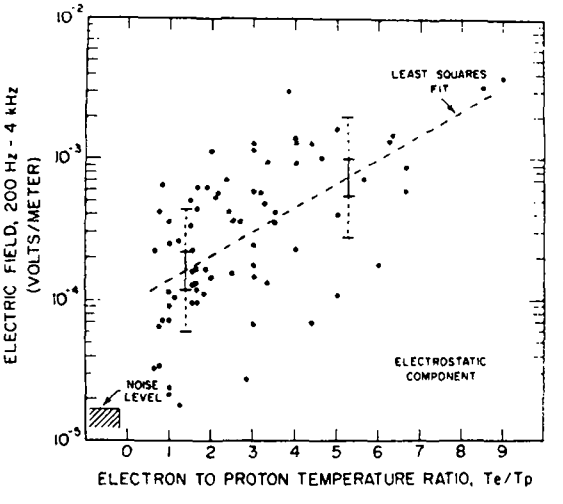

FIG. 5*b*. — Plot of $E_{\mathrm{rms},1}$ against T_e/T_p, which indicates a positive correlation. The correlation between $E_{\mathrm{rms},1}$, which is the rms field strength of the electric field between 20 and 200 Hz in the shock spectrum, and T_e/T_p is observed to be similar to that between $E_{\mathrm{rms},2}$, and T_e/T_p, shown in *a*. The error bars have the same meaning as in *a* [12].

scatter of the data points can be understood if we note that the authors have not considered the dependence of the electrostatic noise amplitude from other upstream plasma parameters such as the Mach number.

The classification scheme adopted commonly in the literature today is based on the observations presented above and it is summarized in figure 6.

First of all the value of $\widehat{Bn}$ tell us if a shock falls in the category of quasi-parallel ($\widehat{Bn} \lesssim 45°$) shocks or of quasi perpendicular shocks ($\widehat{Bn} > 45°$). For quasi perpendicular shocks we have to distinguish between at least the following four cases :

1) $\beta \ll 1, M < M^*$: Laminar shocks : a cold plasma shock with low Mach numbers.

2) $\beta \ll 1, M > M^*$: Quasi-laminar shocks : a cold plasma shock with a high Mach number.

3) $\beta \simeq 1, M < M^*$: Quasi turbulent shock : a warm plasma shock with low Mach number.

4) $\beta \simeq 1, M > M^*$: Turbulent shocks : a warm plasma shock with high Mach number.

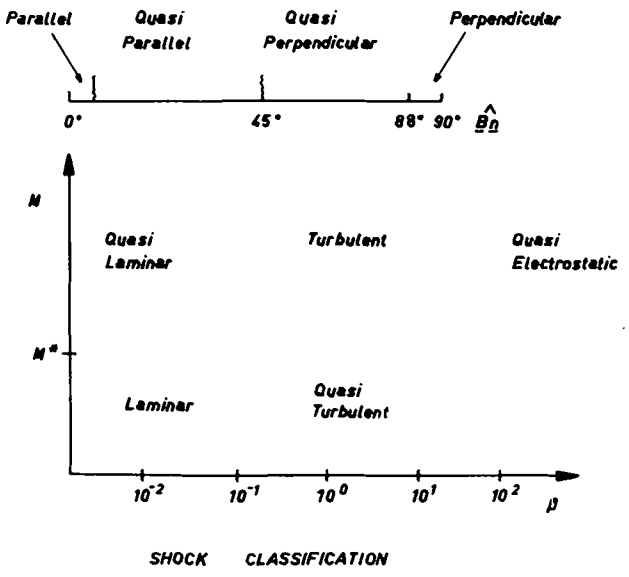

FIG. 6. — Classification scheme for collisionless shock waves based on three parameters only $\widehat{Bn}$, β, M.

Although rather unfrequent, in the solar wind another class of quasi perpendicular shock waves has been reported :

5) $\beta \gg 1$, $M > M^*$: « Quasi electrostatic » shocks : an hot plasma shock with high Mach number.

For quasi parallel shocks the diagnostic available until now does not justify an analogous classification as the *shock structure* is so highly turbulent that it makes the location and identification of the structural elements difficult. It should be noted that there are elements to state that the quasi perpendicular shocks should probably be divided in other subclasses with respect to $\widehat{Bn}$. A first subclass, the object of many theoretical studies, contains the perpendicular shocks $\cos \widehat{Bn} \lesssim \sqrt{m_e/m_i}$; but the oblique shocks themselves (with arcos $\sqrt{m_e/m_i} > \widehat{Bn} > 45°$) may have, in some cases (a certain range of $\widehat{Bn}$ values) upstream features not present for another range of $\widehat{Bn}$ values. This last idea, however, is for the moment only an hypothesis, although supported by some observations.

In conclusion we may give some rough estimates of the probability of finding the earth's bow shock wave in one of the classes listed above. As mentioned previously the geometry is such that $\widehat{Bn}$ ranges almost always over all the 0°-90° range, including therefore parallel, quasi-parallel, quasi-perpendicular and perpendicular shocks. The most probable shocks, however, will be quasi-parallel and quasi-perpendicular. As for M and β, for the four classes listed above a frequency of 1.9 %, 1.6 %, 4 %, 92.5 % respectively has been reported in the solar wind [14], the case with $\beta \gg 1$ being observed only in a very small percentage of cases (< 1 %).

It should be noted that the presence of a 5 % α-particles population has been ignored in most of the literature, only in two papers has the α-particles, behaviour through the bow shock been studied [15], [16]. This limitation is due to the absence of good data of α-particles thermalization accross the shock layer in almost all the flown satellites. Studies like those in references [11], [16], however, have indicated that α-particles may be an important tool in studying the potential drop across the shock layer : an important feature ignored in past studies of the earth's bow shock waves.

3. **Laminar shocks.** — A shock is laminar when no macroscopic turbulence destroys the smooth profile of the plasma parameters. The shock wave will appear as a continuous coherent change in the plasma distribution and in the field profile. If the turbulence is completely absent the shock itself will not exist and only solutons or infinite wave trains are found theoretically. To introduce dissipation in the shock, so to have an irreversible transition from upstream to downstream, a microturbulence has to be assumed in the shock layer. Clearly the wavelengths present in the microturbulence should be all much smaller than the shock thickness. This is the main theoretical limitation for laminar shocks, therefore laminar shocks were found theoretically, also in the high β plasma and with Mach number relatively high. Experimentally it appears that laminar shocks can exist only for a cold plasma with low Mach numbers ($M_A < M^*$).

3.1 OBSERVATIONAL FEATURES. — Laminar shocks in space were first identified on the basis of the downstream plasma and magnetic field state. In reference [17, 18] it has been shown that the downstream magnetic field, in cases of low β and low M upstream, had no memory of the shock turbulence, the opposite

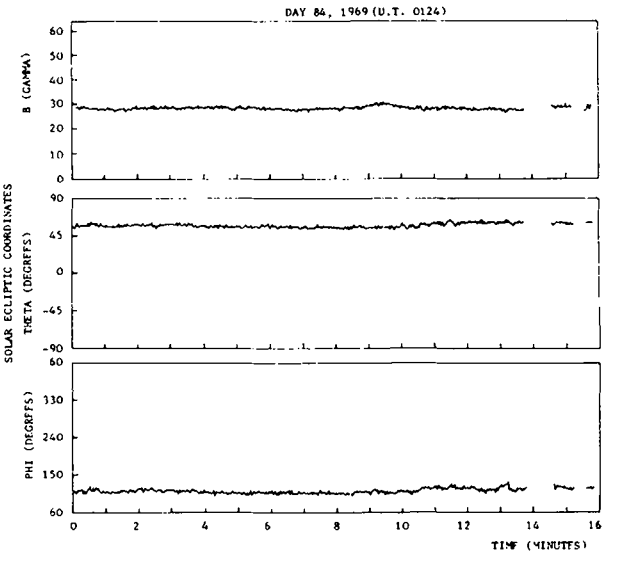

FIG. 7. — Magnetosheath magnetic field intensity B latitude θ and longitude Φ, observed by HEOS-1 downstream of a laminar shock structure on Day 84, 1969 [18].

being true in all the other cases (see the magnetic field intensity B, longitude φ and latitude θ for day 84, 1969 (Fig. 7) compared with similar data for a turbulent shock case shown in figure 19).

Furthermore the particle velocity distribution was Maxwellian both downstream and upstream, while for high Mach numbers ($M > M^*$) the distribution is not Maxwellian in the sense that a long high energy tail is observed : in figures 8, 9 four energy spectra observed downstream of four different shock structures are compared : the data points (black dots with error bars) have been fitted with the distribution

$$f_K(\vec{w}) = \frac{K\,!}{K^{3/2}[K - (\frac{3}{2})]\,!\,\pi^{3/2}\,W^3} \times \times \left[\left(1 + \frac{|W|^2}{KW^2}\right)^{K+1}\right]^{-1} \quad (2)$$

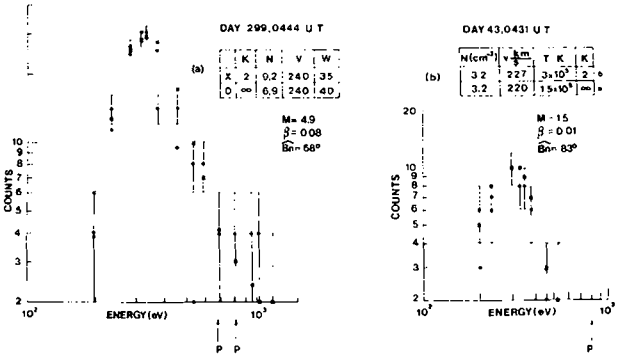

FIG. 8. — Proton energy spectra measured by HEOS-1 downstream of shocks with $\widehat{Bn} > 45°$ and $\beta \ll 1$. Day 299 spectrum has $M > M^*$ and shows a long high energy tail (quasi laminar structure), while Day 43 spectrum has $M < M^*$ and shows a Maxwellian distribution (laminar structure). Arrows on the bottom of the figure indicate the energy channels where protons were observed upstream of the shock [23].

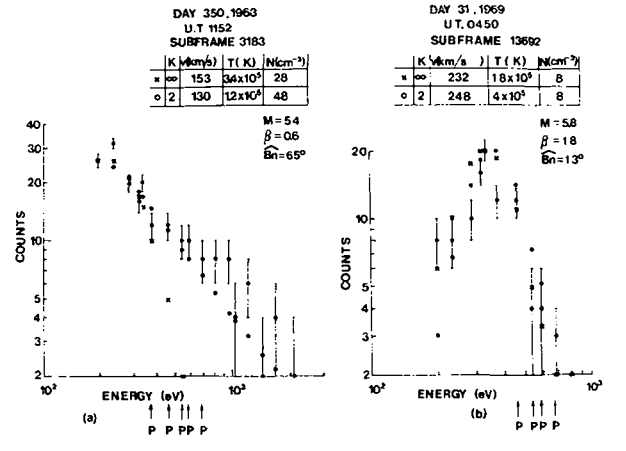

FIG. 9. — Proton energy spectra measured by HEOS-1 downstream of shocks with $\beta \simeq 1$ and $M > M^*$. Day 360 spectrum has $\widehat{Bn} > 45°$ and shows a long high energy tail (quasi perpendicular structure), while Day 31 spectrum has $\widehat{Bn} < 45°$ and shows a Maxwellion distribution (quasi parallel structure). Arrows on the bottom of the figure indicate the energy channels where protons were observed upstream of the shock [23].

where W is the proton thermal speed and $K \geqslant 2$ is a parameter that for a Maxwellian distribution goes to infinity (f_∞ is the Maxwellian). Downstream of a laminar shock (Fig. 8*b*) the distribution is still Maxwellian, in agreement with theoretical expectation.

A complete multidiagnostic view of two laminar shocks is shown in figure 10, taken from the detailed study of quasi-perpendicular laminar bow shock structures presented in reference [19]. The magnetic field shown at the bottom of figure 10, was sampled at 0.144 s apart, which was adequate to provide 67 measurements in the ramp alone. The two shock profiles are very similar, although they are separated in time by 30 minutes ; the three magnetic components, not shown in the figure, were equally laminar. Each of the two shock signatures shows a *plume* consisting of five distinct waves, or pulses, at the top of its main field jump. The time dimensions of the main ramp are respectively 4 s and 5.15 s, corresponding to 2-3 c/ω_{pi}. Similar dimensions have the plumes, whose importance is at the moment unclear. In figure 10 the range of estimated c/ω_{pi} thickness is noted. Above the magnetic field intensity the plasma integral flux profile is shown in figure 10, as observed by the JPL Faraday cup. This analyzer maintained a fixed view toward the sun, with acceptance angle determined by 50 % transmission at 20° and zero near 40° ; absence of flux downstream of the shocks signifies deflection of flow outside the acceptance angle of the instrument, at left and right edges, respectively, in the figure. Within the ramp, the flux inderwent some small fluctuations as the shock was approached, then a series of major oscillations began just as the ramp started. These oscillations are identified by numbers 1 through 5 in both shocks. Finally the flux reappeared at a very low level behind the shock due to deflection of the bulk velocity. The pattern of major flux oscillations was evidently a fixed characteristic of the laminar shock structure, as the numbered maximuns and minimums in the two panels elucidate. Note that the flux peaks should be interpreted as density increase in the sheath side half of the shock ramp.

The third and fourth graphs from the bottom of figure 10 illustrate the relative thermal behaviour of solar wind electrons and protons, in uncalibrated telemetry units. The shaded portions of the electron retardation curves (University of London Longmuire probe) indicate the difference between those spectra and the un affected solar wind distribution measured upstream several minutes outside the shock. The right panel show that significant enhancement at high energy took place in the first half of the ramp ; the left panel shows that full thermalization had practically occurred by the end of the ramp. The Lockheed light ion spectrometer (fourth graph) peered in a direction not aligned with the sun and therefore detected only thermalized protons that moved in direction accross the original direction of flow.

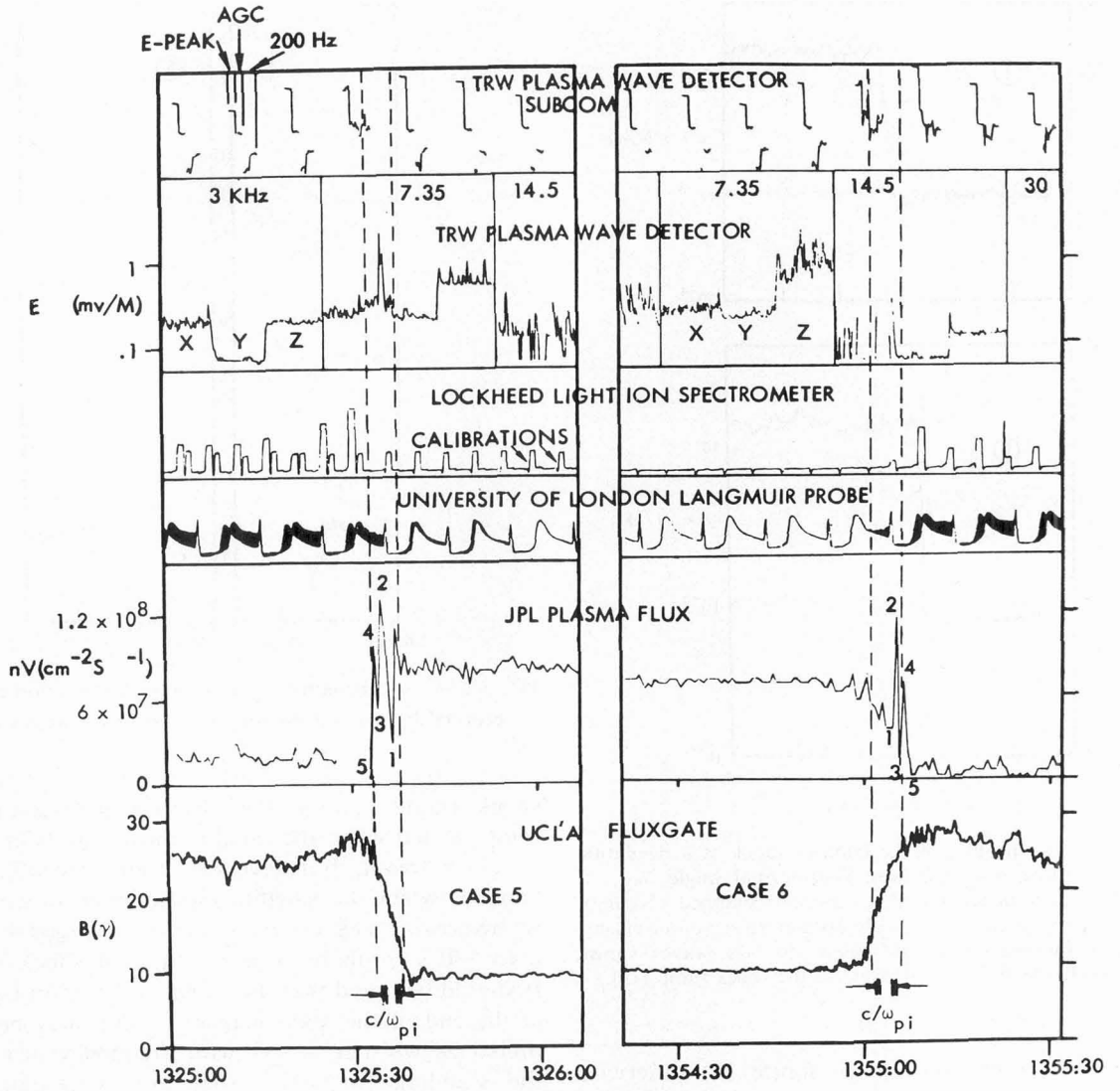

FIG. 10. — Multidiagnostic view of two laminar shock crossings : See text for further exploration [19].

The left panel shows, then, that by midramp no proton thermalization whatever was apparent, while, from the right panel, some proton heating could have occurred after midramp. By the end of the plume both protons and electrons where deflected and thermalized. The sequence of observed plasma events in the laminar shock was, then, as follows : early deflection of flow and start of thermalization of electrons, strong variations in density and start of thermalization of protons, unreduced bulk velocity through most of the field ramp until the flow was redirected and the antisolar flux component was so diminished at the head of the ramp that plasma parameters could no longer be determined by the J. P. L. Faraday cup.

Electrostatic noise data are presented in the fifth and sixth graph on the top of figure 10. Although the T. R. W. Plasma wave detector was not in the most favorable channel, a well defined spike of 7 kHz noise was recorded at midramp simultaneously with the forward edge of the major density elevation in the left panel, and a noise jump at 14 kHz was detected at the analogous point of the right panel. In the sixth strip we see that in both panels the 200 Hz channel recorded increase in noise level outside the ramp where the electrons were already affected by the presence of the shock and that the 200 Hz noise was considerably elevated where partial thermalization of the electrons was taking place, both early and late, in the ramp. This behaviour of the 200 Hz plasma wave noise is confirmed in figure 11 for two other laminar crossings of the same satellite OGO-5 in the same day. The electrostatic noise is strictly confined to the shock ramp if no standing waves

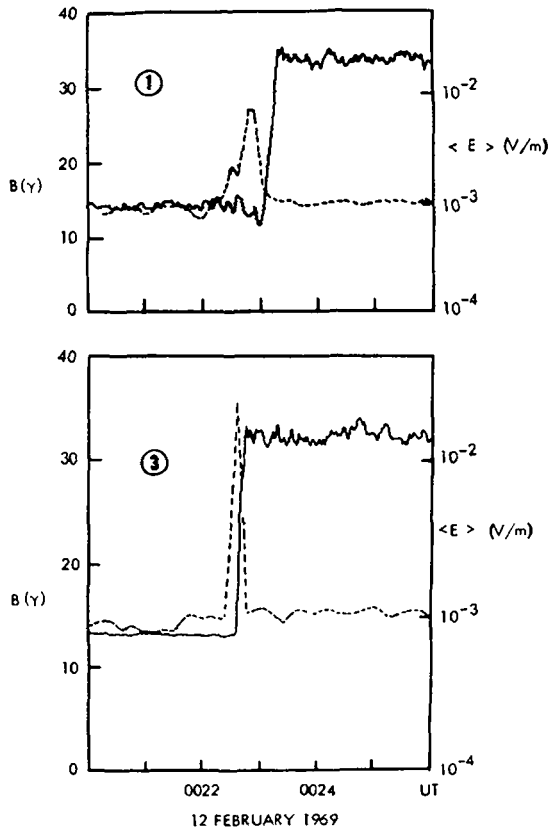

FIG. 11. — Two profiles of the laminar shock at a resolution of 1.15 s/sample, with differing field-normal angle θ_{nB}. At $\theta_{nB} \approx 65°$, upper panel, the shock exhibits damped precursor oscillations, with a correspondingly broadened region of plasma wave noise (dashed curve). At $\theta_{nB} \approx 78°$, the waves vanish and the electric noise is narrowed to the shock ramp [19].

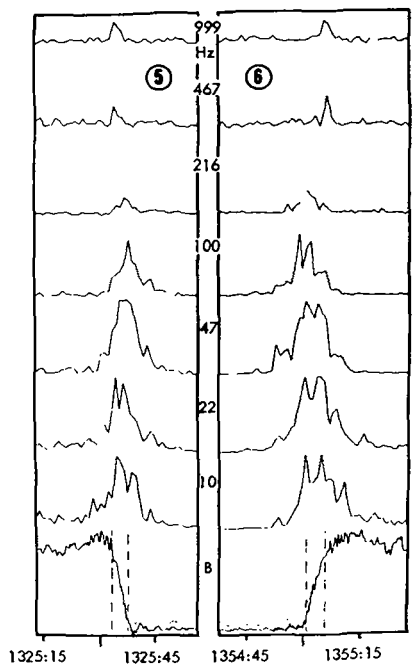

FIG. 12. — Multi-channel view of the high-resolution crossings as recorded by the X-axis loop of the $\dot{B}$ ELF search coils [19].

are present (at the bottom in figure 11) otherwise the plasma wave noise may broaden over all the standing precursor.

The electromagnetic noise also observed in the two shock crossings of figure 10 is shown in figure 12 with the field magnetic profile repeated at the bottom for reference. Individual channel center frequencies are identified in the vertical center column between the two panels. Electromagnetic wave noise began upstream from the ramp concurrently with the appearance of the small damped standing waves ahead of the shock, shown in figure 11, and continued through the ramp. This upstream noise had an upper frequency cutoff between 216 and 467 Hz : the electron gyrofrequency was $\Omega_e \simeq 252$ Hz. Figure 12 therefore represents whistler mode noise arising in the shock and propagating at an angle less than 60° to $\bar{B}$ since the high frequency whistler cutoff becomes 216, 100, 62 Hz respectively for propagation at 30°, 60°, 75° to $\bar{B}$. The low frequency end of this noise is probably revealed by the satellite as standing whistler waves (see Fig. 11). These standing whistlers have been extensively studied in reference [20]. These authors have confirmed that the waves were standing in the shock frame because the observed polarization was right-handed when the satellite moved from upstream to downstream, but reversed itself, becoming left-handed, when the satellite moved from downstream to upstream. The observed period changed between 6 to 130 s. probably due to different shock speeds. It should be noted that the *plume* observed in figure 10 at the end of the main magnetic ramp may be interpreted as whistler waves with frequency just below the standing frequency, that are being convected downstream.

In concluding this section on the observations of laminar bow shock structures, it should be noted that unlike laboratory experiments, the presence of an electrical potential barrier at the laminar bow shock has not been established, although it has been suggested for high M high β shocks [2, 6]. Another important feature, still unclear, is the possibility, for oblique ($\widehat{Bn} \leqslant 45°$) laminar shocks to reflect (and accelerate) protons so to generate the kind of upstream wave phenomena observed for quasi parallel high β high M collisionless bow shock. In reference [21] ≈ 1 Hz waves usually related to backstreaming electrons, have been observed [20] ; lower frequency waves, related to backstreaming ions, have never been reported.

3.2 COMPARISON WITH THEORY. — The theory of collisionless laminar shocks is one of the more deeply developed and allows a detailed comparison with observations. In the approximation of zero temperature plasma the solution of shock equations [8] provides solitons (solitary wave pulses) and infinite wave

trains both for perpendicular and oblique propagation. Neither of these two solutions, however, is a shock in the sense that the waves do not dissipate the ordered upstream energy. Finite temperature effects, however, introduce dissipation and allow one to construct the fine structure of the shock wave. The shock structure will depend on the relative importance of the dispersion effects (length) with respect to the dissipation length. For quasi perpendicular shocks (propagating at large angles to **B**) the magnetic field gradient in the wave is so large that the electric current may provide dissipation through resistivity. Laminar shocks are, indeed, also called resistive shocks. Classical resistivity, however, is not enough to provide dissipation, therefore the problem is to see if the current intensity is high enough to exceed the critical value for excitation of waves that may cause an anomalous resistivity and therefore may dissipate the ordered energy. Depending on the strength of the anomalous resistivity the shock structure will be monotonic or oscillating in the case of small or large dissipation length respectively. Which of the many possible current driven instabilities (Langmuir waves, ion sound, ion cyclotron, electron cyclotron, longitudinal oscillations of magnetized electrons, etc.) will then control the low Mach number cold plasma shock ? Theoretical considerations allow us to conclude [6] that for perpendicular shocks in low β plasma at the initial portion of the shock front, the current threshold for very strong instabilities such as Buneman or Bernstein modes are exceeded even in initially isothermal plasma. These strong instabilities heat preferentially the electrons, and the ion sound instability with the lowest current threshold would stop the magnetic field profile steepening at a level where other instabilities do not grow. The effect of the unstable waves is included in the effective plasma conductivity and the magnetohydrodynamic equations can be reduced to a generalized Ohm's law at least for the magnetic field profile [7].

The shock thickness is then computed in the limit of quasi linear approximation for the waves present in the shock :

$$\delta_{QL} = \frac{c}{\omega_{pi}} \left(\frac{m_e}{m_i}\right)^{1/4} \frac{(M^2 - 1)}{\sqrt{\beta_e}}$$

for

$$(M^2 - 1)^2 \frac{B_0^2}{4\pi} n_0 c(m_i T_e)^{1/2} < A \left(\frac{m_e}{m_i}\right)^{1/4} \tag{3}$$

or in the limit of non linear approximation (strong turbulence) for the waves [6] :

$$\delta_{NL} = \frac{c}{\omega_{pi}} \left| A \frac{m_e}{m_i} \frac{c(M^2 - 1)}{\beta_e V_A} \right|^{1/3} \tag{4}$$

for

$$A \left(\frac{m_e}{m_i}\right)^{1/4} < (M^2 - 1)^2 \frac{B_0^2}{4\pi} n_0 c(m_i T_e)^{1/2} < \left(\frac{m_e}{m_i}\right)^{1/2}.$$

For more oblique propagation, however dispersion effects may become important as the dispersion length

$$L_d = \frac{c}{\omega_{pi}} \frac{(\pi/2 - \widehat{Bn})}{(M^2 - 1)^{1/2}} \tag{5}$$

may become so large that the magnetic field profile steepening is stopped and the dissipation occurs in a length larger than L_d

$$\delta = 4\pi L_d^2 \sigma_{eff}(M^2 - 1) \frac{V_A}{c^2} = \frac{L_d^4}{(M^2 - 1)} \frac{\omega_{pi}^4}{c^4} \frac{C_S^2}{A V_A \omega_{pi}} \tag{6}$$

the shock being therefore oscillating.

The observed features of the laminar structures agree qualitatively with the theoretical results. Electrostatic noise is indeed observed in the shock layer (Figs. 10, 11), concentrated at midramp, and is probably responsible for proton thermalisation. Greenstadt *et al.* [19] have shown that the condition for generation of electrostatic ion acoustic waves in the shock were probably satisfield in the cases shown in figure 10. Also the measured shock thickness in reference [19] appears to be in agreement with the value computed from 3, being a few times c/ω_{pi}. It should be noted, however, that a detailed study of the shock thickness as function of $\widehat{Bn}$ has not been published until now because of the mentioned difficulty about the unknown shock speed.

An important agreement between the theory and the observations has been found for the whistler waves standing in front of the shock. Most of the observed laminar shocks, indeed, had values for

$$b_x = \frac{\cos \widehat{Bn}}{M_A} \quad \text{and} \quad b_z = \frac{\sin \widehat{Bn}}{M_A} \tag{7}$$

such that in the classification of Tidman and Krall [8], p. 83, Figs. 5.3) they corresponded to four imaginary roots to the shock equations, i. e., corresponded to solutions in which the stationary whistler played an important role. The wavelength and amplitude were given by ([8], p. 159)

$$K \simeq \frac{\omega_{pi}(M_A^2 - 1)^{1/2}}{c \cos \widehat{Bn}} \tag{8}$$

and

$$\frac{\Delta B}{B} \simeq a \cos \widehat{Bn} \left| \frac{\beta}{(M_A^2 - 1)} \right|^{1/2}. \tag{9}$$

In eq. (9) the constant « a » changes with T_e/T_i, being $a \simeq 21.4$ for $T_e = T_i$, and $a = 0.7$ if $T_e \gg T_i$. In ref. [20] eq. (9) has been experimentally controlled (Fig. 13) and a value $a = 3.7$ has been found for the solar wind, where T_e is larger than T_i but not too much larger. The agreement with the theory was good also when no standing whistler was observed ($\Delta B/B \simeq 0$).

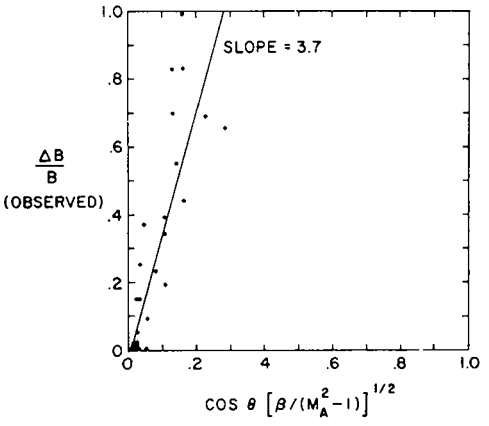

FIG. 13. — Comparison between the observed amplitude of the standing whistler waves and the theoretical prediction evaluated using measured upstream parameters [20].

4. **Quasi laminar shocks.** — When the Mach number of a cold plasma shock is increased, the anomalous resistivity will reduce the steepening of the magnetic field profile, but will not reduce the steepening of the particle parameters profile. The ion density and velocity wave, for example, may steepen and break much earlier than the magnetic intensity. The consequence of the breaking of ion plasma parameters is the generation of counter streaming particles, and eventually, of quasi trapped ion orbits. Counter streaming particles will provide the viscosity needed for ion thermalization, in a thin layer (called subshock) that may be of the order of the Debay length thick. Further increasing the Mach number, wave breaking will occur also for the field intensity profile, and the shock will lose all its laminar aspects.

In the low β case with $M_A > M^*$ the collisionless shock wave, therefore, will show some properties typical of the laminar shocks, namely the absence downstream of low frequency turbulence in the magnetic field intensity, but new features in the plasma properties and in the electrostatic noise should be present.

4.1 OBSERVATIONAL FEATURES. — The quasi laminar downstream plasma state was first studied in reference [22]. The authors noted a magnetic field intensity with no turbulence downstream of a shock with $\beta \ll 1$ and $M_A > M^*$. The ion velocity distribution, however, was different from the upstream Maxwellian, having a distribution with long high energy tail, corresponding to $K \simeq 2$ in eq. (2). Figure 8 shows an energy spectrum observed on Day 299, 1969 downstream of the quasi laminar shock studied in ref. [22] : the best fit to the data is given by a $K = 2$ distribution (crosses) not by a Maxwellian ($K \simeq \infty$, open circles). An interesting detail evident in figure 8, is that some particles observed downstream had an energy higher than the energies observed upstream (indicated with arrows and « P » in the figure) : some particles underwent actual acceleration in the quasi laminar shock.

An important feature noted in references [21, 22] is the magnetic field intensity oscillations downstream of the quasi laminar shocks. These oscillations have been observed many times also with other satellites.

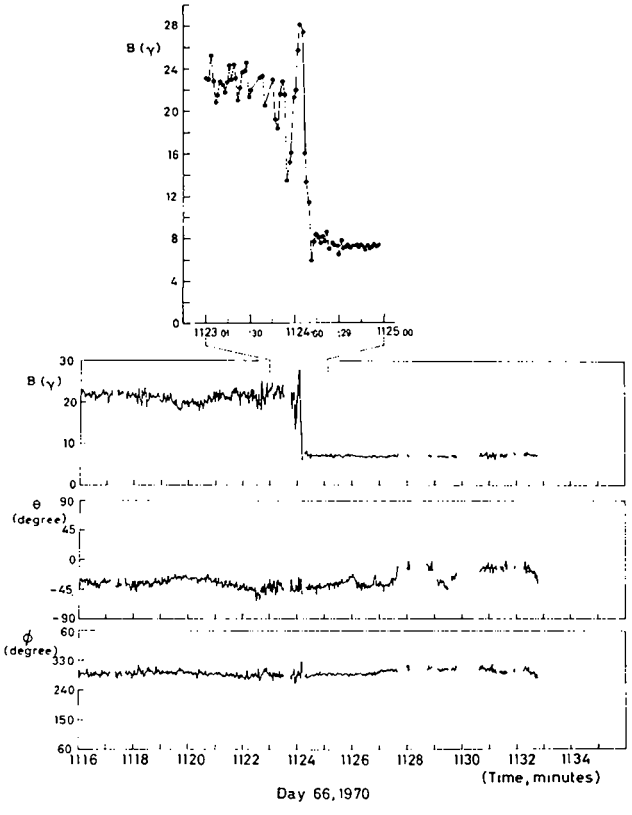

FIG. 14. — Magnetic field data for the quasi laminar bow shock structure observed by HEOS-1 on Day 66, 1970. Single measurements of B across the shock are shown at the top. The polar latitude θ and longitude Φ are in GSE coordinates [21].

Figure 14, taken from reference [21], illustrates this feature : after the first magnetic ramp, during which B raises from 7 to 27 γ, the intensity decreases to 13 γ and then through oscillations of decreasing amplitude reaches the downstream value of 23 γ. It is clear that the dissipation length is in this case longer ($\simeq$ 4 times) than the dispersion length. An important difference, with respect to laminar shocks, however, is the fact that the oscillations are present downstream of the main ramp, not upstream as in figure 11. This fact confirms that the structure of the shock is different from the low Mach number case. The location of the oscillations indeed, tells us if within the shock the noise present has a $d\omega/dK$ increasing or decreasing : if $d\omega/dK$ is increasing in the dispersion region, energy can be transferred, through mode coupling to higher frequencies which will run ahead of the main pulse and damp out upstream (as in laminar shocks), whereas if $d\omega/dK$ is decreasing they trail the main pulse and damp out downstream (as in quasi laminar shocks).

More information on quasi laminar shocks has been obtained with OGO-5 data in reference [23], [24]. In the *catalogue* of bow shock observations [23], the authors have shown that intense electrostatic noise is observed also in quasi laminar shocks. In figure 15 is shown an example of detailed quasi laminar structure observed by OGO-5 on day 348, 1969. The diagnostic available are : the magnetic field, electrostatic noise, Langmuir probe data and the electromagnetic search coil data. The magnetic profile, shown on the top of figure 15, shows, again as in figure 14, damped oscillations downstream of the main ramp. The plasma wave detector measured 1.3 kHz in the first part of the main ramp and 3 kHz in the last portion of the ramp and during the oscillations. The noise is more intense in 1.3 kHz band (the ion plasma frequency was $\simeq 720$ Hz) and appear to radiate ahead of the main ramp together with small amplitude whistler noise. In the middle of the ramp bursts with amplitude up to 70 mV/m are observed. The 3 kHz noise is observed in the last portion of the ramp, then, when B starts decreasing, the amplitude of the electrostatic noise drops by a factor 10 and slowly disappears ; when it reappears, at the second pulse, it seems to have lower intensity. The Langmuir probe clearly shows that for the end of the main ramp the electrons have been completely heated. The electfromagnetic noise data, shown in figure 16, with the magnetic field profile on the top, is clearly limited to the main ramp and only at low frequencies appears to be present somewhat ahead of the ramp itself.

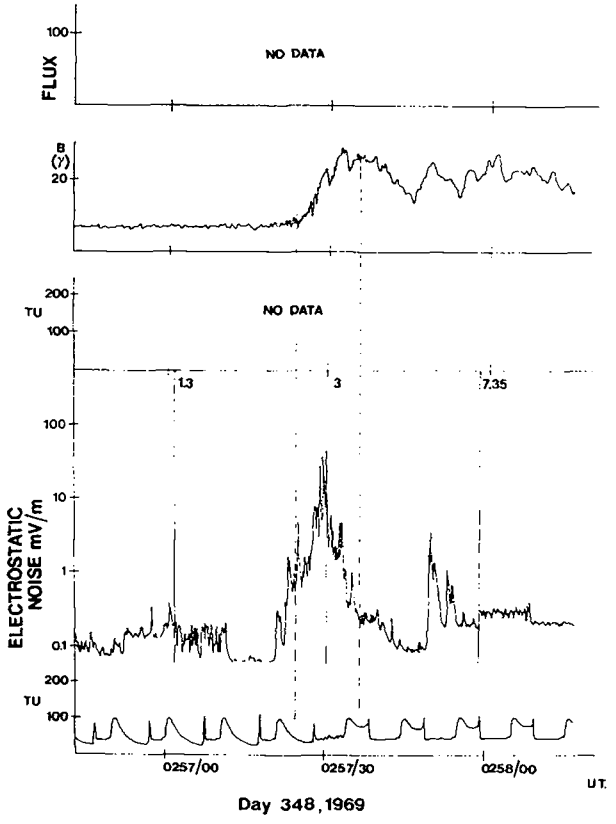

FIG. 15. — Multidiagnostic view of a quasi laminar shock structure observed by OGO-5 on Day 348, 1969. From the top are shown : positive ions integral flux (No Data) in arbitrary units ; magnetic field intensity profile (in gammas) ; Lockheed light ion spectrometer (No Data) ; electrostatic noise in μV/m in seven frequency bands (0.56, 1.3, 3, 7.35, 14, 30, 70 kHz) ; and the electron distribution langmuir probe measurements (one every 10 seconds). The two vertical dashed lines locate the main magnetic ramp [23].

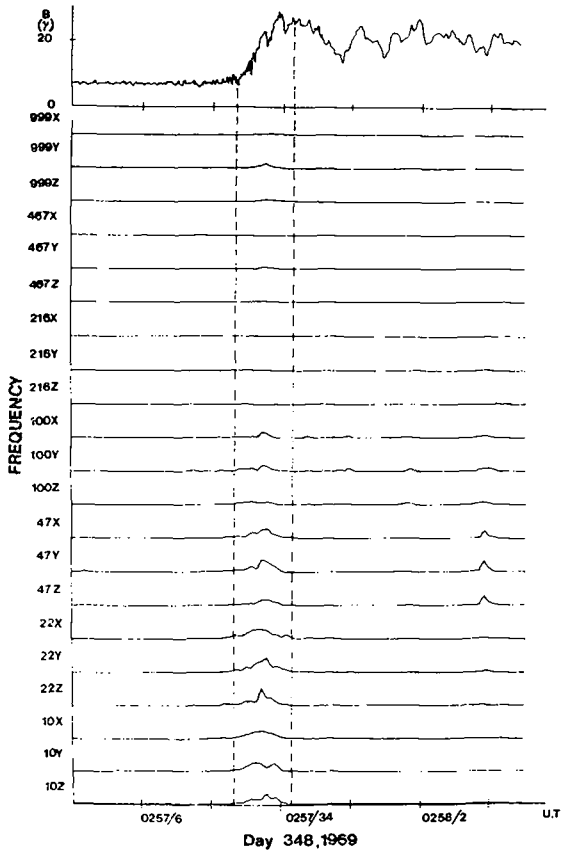

FIG. 16. — Electromagnetic noise data for the same shock structure shown in figure 15. The magnetic field profile is shown on the top for reference. Three axis intensity data are shown, for each of the seven frequency band (10, 22, 47, 100, 216, 467, 999 Hz) explored, in arbitrary units [23].

No more experimental information is available for this structure of the earth's bow shock, the probability of its observations being rather low. Observations of oblique ($\widehat{Bn} \lesssim 45°$) shocks with $M > M^*$ and $\beta < 1$ have been reported (see [35] below) but will be discussed in the quasi parallel structure section, as when $\widehat{Bn} \lesssim 45°$ the influence of M_A and β appear to be negligible.

4.2 COMPARISON WITH THEORY. — The comparison of quasi laminar structure observations with theoretical results is difficult because of the incompleteness

and poor quality of the observations, and because of the lack of complete theories.

As we have mentioned above, when the Mach number is increased in a low β shock, the thickness of the shock tends to increase (see eq. (3)) while the magnetic profile steepening is prevented by the anomalous resistivity. The breaking of the plasma density and velocity profile introduces counter streaming of particles, therefore generates viscosity in a thin layer (a *subshock*) that should quickly heat the ions and generate electrostatic turbulence. This turbulence irradiates upstream and downstream of the subshock ; the incoming ions will, then, spend enough time in this turbulence to undergo stochastic acceleration. At the subshock, therefore, there will be suprathermal particle generation. These particles will have enough energy to move upstream, generating a *foot* in front of quasiperpendicular shock structure and a long precursor in front of quasi parallel shocks. The *foot* has been observed in laboratory experiments [2] and has a length of the order of c/ω_{pi}. In space observations the presence of the *foot* for quasi laminar shocks is not clear and may, perhaps, be recognized in figure 14, but not in figure 15. The presence of a subshock is not evident in the observations, although there is evidence of intense electrostatic noise over a range larger than the main ramp (Fig. 15), and of ions accelerated to energies higher than upstream energy, to generate the long high energy tail observed in figure 8. As for the laminar shock case, no information is available for the electric potential drop across the quasi laminar shock, although theoretically it plays a very important role in the breaking of ion motion. This potential drop has been observed in laboratory experiments [25] to increase above $M_A \simeq 3$, have a maximum at $M_A \simeq 4$-5 and then decrease again to zero for $M_A \simeq 7$.

It should be noted that a collisionless shock wave does not leave the particles velocity distribution necessarily unchanged. If the distribution is Maxwellian upstream and downstream, then [8]

$$\int d\bar{v}v_x < \delta f^2 >_2 = \frac{N_1 V_1}{2\sqrt{2}(2\pi)^{3/2}} \left(\frac{N_1}{W_1^3} - \frac{N_2}{W_2^3}\right) \quad (9)$$

where δf is the fluctuating part of the particle distribution function ; N, V, W are density, bulk speed and thermal speed respectively. For high Mach number the right hand term in eq. (9) is positive and large, meaning that a large amount of shock turbulence is needed for obtaining a Maxwellian distribution. As the ion velocity distribution downstream of quasi laminar shock is not Maxwellian, it follows that the classical Rankine-Hugoniot relations are not valid for this shock structure, because these relationships make use of the assumption of a Maxwellian velocity distribution on both sides of the discontinuity.

5. **Quasi turbulent shocks.** — A shock with a low Mach number ($M < M^*$) and high β ($\beta \gtrsim 1$) has been called, in Section 2, *quasi turbulent*. The fact is that not too much information is available (both theoretically and experimentally) on this kind of structure. Theoretically it is said that in a very high β plasma, ion waves should propagate faster than magnetosonic waves, therefore they should dominate the shock structure. Here we are dealing, however, with $\beta \gtrsim 1$. Can a shock with $M_A < M^*$ and $\beta \gtrsim 1$ be resistive, and, therefore, laminar ? Theoretically we may argue that if β increases the dispersion length increase [26], therefore the magnetic gradient decreases, and the electric current may decrease below the threshold for the instabilities involved in anomalous resistivity. The magnetic gradient decreases, also, with increasing Mach number ; it is therefore clear why the resistive shocks in high β plasmas can exist for M only slightly larger than 1 (see Fig. 2). Within the shock ramp, however, β increases still further ; there is, then, the possibility of strong mode coupling between ion sound waves and whistler waves as it has been suggested in reference [26].

This coupling will transfer energy from electrostatic modes to electromagnetic modes, and certainly an intense electromagnetic noise should be observed, as electromagnetic waves are more easily detectable.

5.1 Observations. — As stated earlier not too many observations of this structures are available. One possible quasi turbulent shock was observed in reference [27] with OGO-5 on March 5, 1969 : the upstream Mach number was $M \approx 3$, $\beta = 2$, $Bn \simeq 46°$. The location of the satellite was such that M may actually have been lower than M^*, although this is not completely certain. The important features were : intense electromagnetic noise observed within the shock ramp and downstream at all frequencies, but with a peak at 100-200 Hz. Also at 200 Hz, and only around this frequency, electrostatic noise was observed. As we shall see in the next section in all the high β plasma shocks the electrostatic noise has a peak at a much higher frequency.

Similar observations have been reported in reference [23].

Day 84, 1969 shock crossing, shown in figures 17 and 18 is one of these. Due to the lower bit rate of the satellite OGO-5, these observations have less measurements per minute, therefore some of the details may have been missed. The shock crossing was observed at 0929 U. T. and in the magnetic field intensity profile, shown in the second strip from the top in figure 17, appears similar to a laminar shock in the sense that downstream there is absence of low frequency magnetic noise. Due to the low sampling rate the Langmuir probe and the Lockeed light ion spectrometer are not able to reveal the details of the thermalization process occurring in the magnetic ramp. The ion integral flux, shown on the top of the

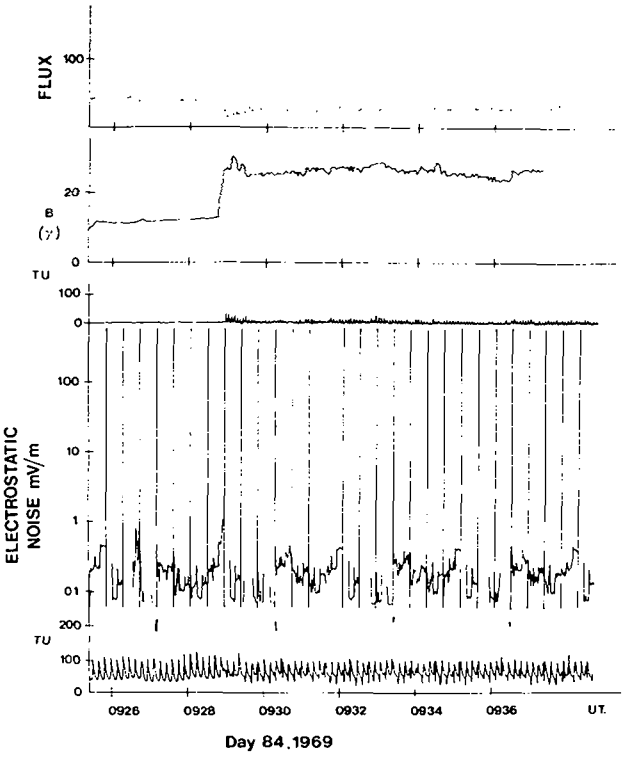

FIG. 17. — Multidiagnostic view of quasi turbulent shock structure observed by OGO-5 on Day 84, 1969. Data are shown in the same format as in figure 15 [23].

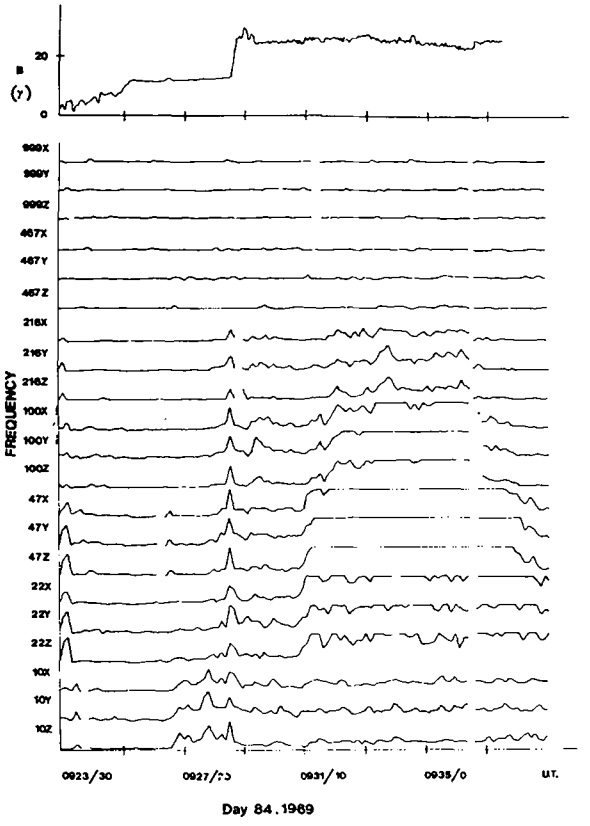

FIG. 18. — Electromagnetic noise data for the shock structure shown in figure 17. Note the presence of intense noise level in the downstream region. Data are shown in the same format as in figure 16 [23].

figure reveals some fluctuations in direction, downstream of the main ramp, in coincidence with some small pulses of B. An important information in figure 17 is contained in the electrostatic noise strip. When the shock was crossed, the satellite was exploring the fourth band of the Plasma Wave Detector series (0.56, 1.1, 3.1, 7, 14, 30, 70 kHz), and a small signal, up to $\simeq$ 1 mV/m, was observed. Note that in other crossings of similar shock structure shown in reference [23], when the second and third frequency band was observed, electrostatic noise with amplitude below 0.5 mV/m was revealed. The low intensity of electrostatic noise in the measured frequencies characterizes this structure as different from the quasi laminar and certainly from the turbulent shock. The electromagnetic noise, shown in figure 18, also characterizes this structure as non-laminar. The electromagnetic noise is present upstream for 2 minutes ahead of the magnetic ramp, within the ramp, and for many minutes also downstream. In the precursor only 10-20 Hz noise is observed. Within the ramp and downstream all frequencies up to ω_{pi} ($\simeq$ 300 Hz in this case) are observed. Note that in figure 18 the downstream noise level increases very much 2 minutes after the magnetic ramp, but in other crossings this increase is absent in the sense that very intense noise level in the magnetosheath side is observed immediately after the magnetic ramp. The high frequency electromagnetic noise is certainly in contrast with the laminar behaviour of the magnetic field intensity profile.

6. **Turbulent shocks.** — More than 90 % of the Earth's bow shock observations have been made for upstream $M > M^*$ and $\beta \gtrsim 1$. This kind of structures, therefore, are of great importance in space plasma physics. The understanding of the shock problem under these condition, however, is rather difficult, due also to the absence of good measurements of quantities that can be directely compared with theoretical results. The difficulty is increased by the fact that the upstream Mach number is often so large that wave breaking occurs, while in another $\simeq$ 50 % the wave breaking should not occur although $M > M^*$. The presence of turbulence on the downstream side changes, also, the magnetic profile so that the structural features may be completely hidden and the shock is sometimes thought to be unstable.

6.1 OBSERVATIONS. — Unlike all the other shock structures the magnetosheath plasma downstream of high β high M bow shock has a magnetic field that it is not steady as in the laminar case (Fig. 7) but shows large amplitude waves both in the magnetic field intensity and direction (Fig. 19). Power spectra of the magnetic fluctuations have been presented in reference [28] for plasmas downstream of turbulent

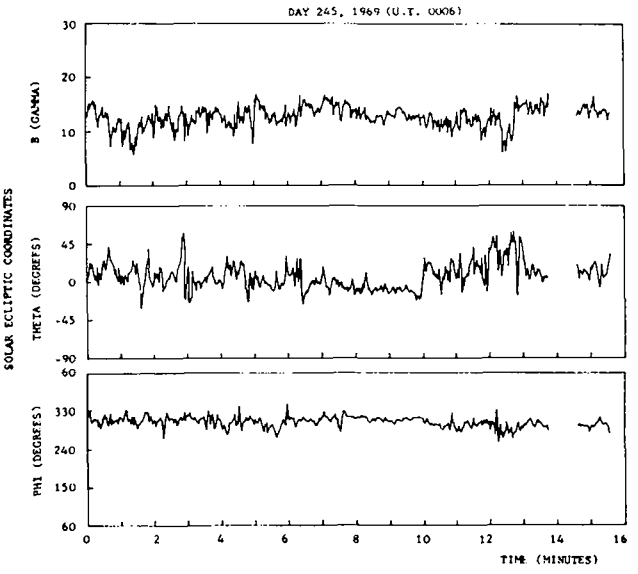

FIG. 19. — Magnetosheath magnetic field intensity B, latitude θ and longitude Φ, observed by HEOS-I downstream of a turbulent shock structure on Day 245, 1969 [18].

shocks : the power spectra slope is $f^{-1.6}$ for $B_{x,y,z}$ and $f^{-1.2}$ for B.

The ion energy spectrum downstream of the turbulent shock shows a long high energy tail (Fig. 9) particles with energy up to 3-5 times the maximum upstream energy are revealed. This fact of a long high energy tail in the ion energy spectrum seems, therefore, to be a characteristic of high Mach number collisionless shocks. How this high energy tail is generated in the shock structure, has been studied in references [29, 30].

Studying quasi crossings of the shock layer, a bimodal ion energy spectrum has been found. In figure 20*a* the magnetic field intensity for one of these

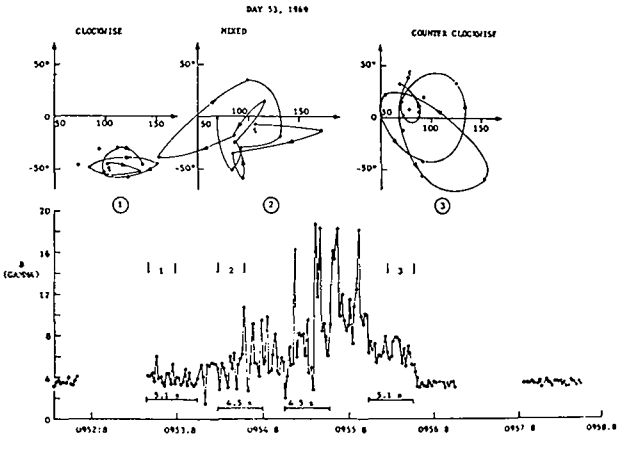

FIG. 20*a*. — HEOS-I single point magnetic field data observed in a quasi crossing of a turbulent shock layer on Day 53, 1969. The magnetic field intensity is shown at the bottom. The polar plots of θ against Φ shown at the top are for the three short-periods marked on the lower plot. At the bottom of the figures are also indicated the average periods of the observed fluctuations [29].

HEOS-I observations is shown together with a polarization study of the waves observed in the structure. Waves in the time intervals « 1 » and « 3 » indicated in the figure, are shown to be standing as they appear to change polarization with changing shock-satellite motion. The simultaneously measured ion energy spectrum is shown in figure 20*b* spectra 2 and 3. These two spectra show, compared with the

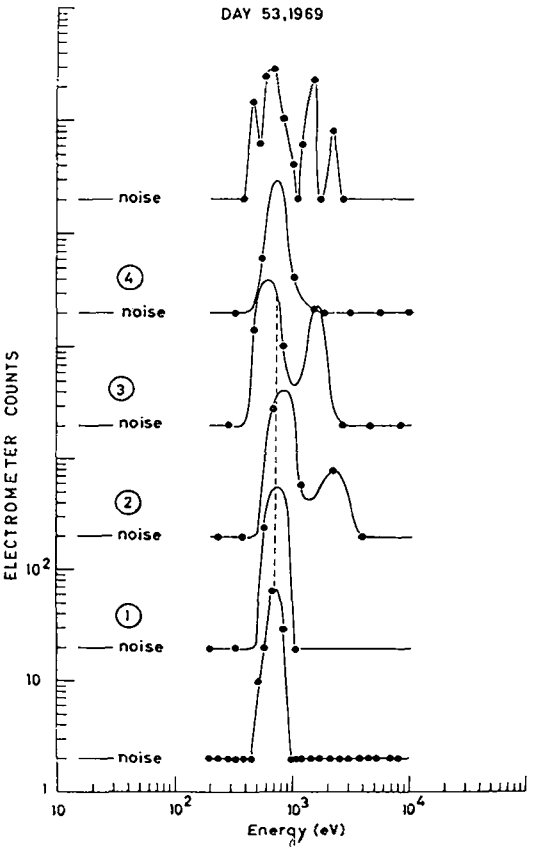

FIG. 20*b*. — Proton energy spectra observed during the quasi shock crossing on Day 53, 1969. The numbers 1, 2, 3, 4 indicate the consecutive four subcycles of the spectrum shown at the top of the figure. The peak of the solar wind proton distribution is marked by the vertical dashed line. The starting times of each spectrum shown are, from the bottom, 09 h 45 m 05 s, 09 h 51 m 29 s, 09 h 53 m, 06 s, 09 h 54 m 43 s, 09 h 56 m 20 s U. T. respectively [29].

unshocked solar wind ion spectrum shown on the bottom of the figure, a second peak at an energy 2-4 times the upstream energy. At the same time the main peak is not thermalized, but only slightly shifted toward lower energies. Only deeper in the shock layer the ions are quickly thermalized and the two peaks are smoothed out to become the high energy tail observed downstream (Fig. 20*c*). Note that the ions in figure 20*b* and *c* are all moving toward downstream, therefore they do not prove the existence of counter-streaming ions.

The ion-ion streaming instability, however, is supported more and more by experimental evidence.

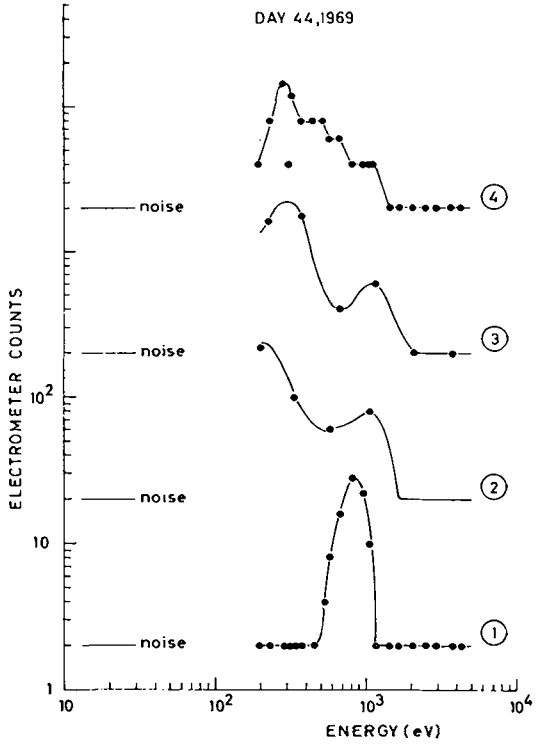

FIG. 20*c*. — Proton energy spectra observed during a turbulent shock quasi crossing on Day 44, 1969. 1) A complete spectrum taken at 01 h 00 m 15 s U. T., 2) and 3) Subcycles taken within the quasi crossing at 01 h 38 m 36 s and 01 h 40 m 04 s U. T. 4) A downstream proton distribution taken at 0217 U. T. [29].

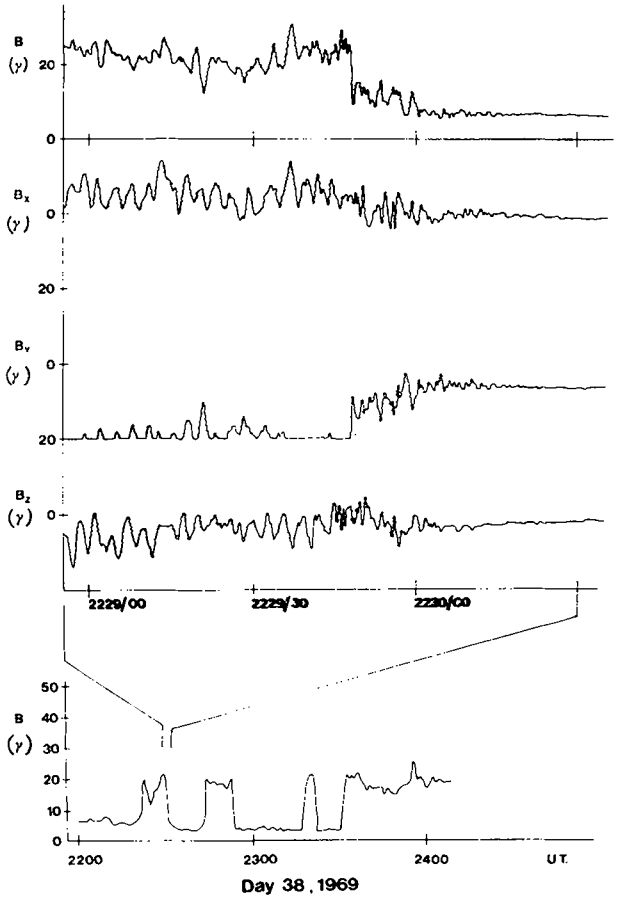

FIG. 21*a*. — A turbulent shock structure observed by OGO-5 on Day 38, 1969. Magnetic field intensity is shown on a compressed time scale (at the bottom) and on an expanded time scale (at the top). Note the double structure at the magnetic shock profile in the expanded time scale [23].

Galeev *et al.* [16] have shown that the thermalization of protons and α-particles are in agreement with the model of ion heating due to two stream instability, and that the resulting potential barrier has a value of the order of one half proton kinetic energy loss, as in laboratory experiments. In ref. [29] it is suggested that the ion heating occurs over a thickness much shorter than the magnetic ramp, suggesting therefore a possible double structure for the shock itself.

Also the magnetic profile suggests a double structure, see figure 21*a* with a long *foot* raising the field intensity from the upstream value to roughly 1/2 the downstream value, and a thin layer where a large increase of B occurs. It is at the beginning of the foot that electrons are accelerated [27] and ions are slightly decelerated [31]. It is also at the beginning of the *foot* that electrostatic noise first appears and reaches high amplitude levels (Fig. 12 [32]), as it is shown in figure 21*b*. In the foot protons are not yet thermalized neither deflected, as it is shown, on the top of figure 21*b*. It is probably in the foot that stochastic electrostatic acceleration may occur, due to the observed electrostatic noise ; the observations shown in figure 20*b*, *c* were therefore taken in the foot of the shock layer. The electromagnetic noise is shown in figure 21*c* : intense bursts of noise are observed downstream and at the thin, large increase of magnetic field intensity. In the precursor only

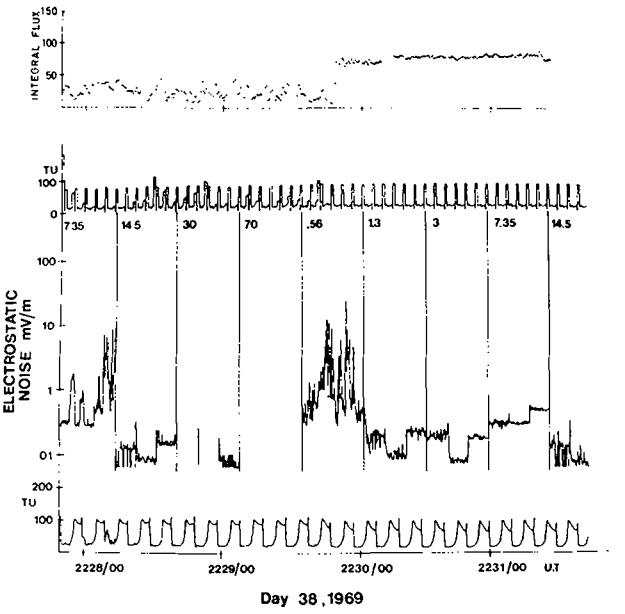

FIG. 21*b*. — Multidiagnostic view of the shock structure presented in figure 21*a*. Data are presented in the same format as in figures 15 or 17 [23].

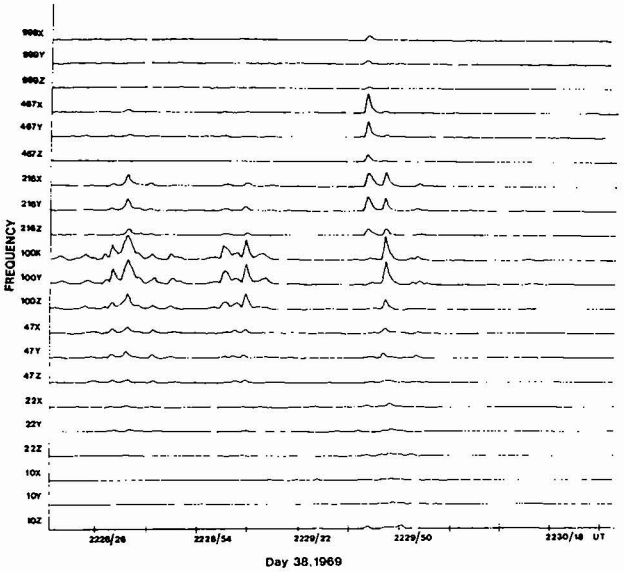

FIG. 21*c*. — Electromagnetic noise data for the same shock crossing presented in figures 21*a*, *b*. Data are presented in the same format as in figures 16 and 18 [23].

VLF noise seems to be present. Note from figure 21 that the shock has to be considered turbulent because electromagnetic noise of all frequencies, electrostatic noise, and the high energy tail in the ion energy spectrum, are observed downstream. The electromagnetic and electrostatic noise spectra have been extensively studied in reference [32].

These authors have found that the electric field spectrum consists of a broad peak typically centered between 200-800 Hz, and of a continuum component decreasing with incerasing frequency as $f^{-(2.0\pm0.5)}$ (Fig. 22). The magnetic field spectrum has only one component decreasing with increasing frequency as $f^{-(4.0\pm0.5)}$; the magnetic field spectrum has also a cutoff at the electron gyrofrequency (Fig. 22). The electric to magnetic energy density ratio of the continuum is about 10^{-3} to 10^{-4} (whistler wave noise), while for the broad peak the ratio is 10^2 to 10^3, i. e. purely electrostatic waves. In figure 5*a* (taken from [12]) it has been shown that both low frequency and high frequency electric noise amplitude increases with T_e/T_i. The electromagnetic noise, on the contrary has a different behaviour at low and high frequencies. In figure 3 we have shown that this noise below $\simeq$ 1 Hz decreases with increasing $\widehat{Bn}$, at high frequency, however (Fig. 23) the noise behaviour is the opposite : increases with increasing $\widehat{Bn}$ this high frequency noise also increases with increasing solar wind density.

A study of the spectral changes through the shock layer has been presented in reference [12] (Fig. 24). Using Imp 6 data these authors have studied in detail the shock crossing shown in figure 24*a*, where magnetic field intensity and direction is shown at the bottom, while on the top of the figure electrostatic

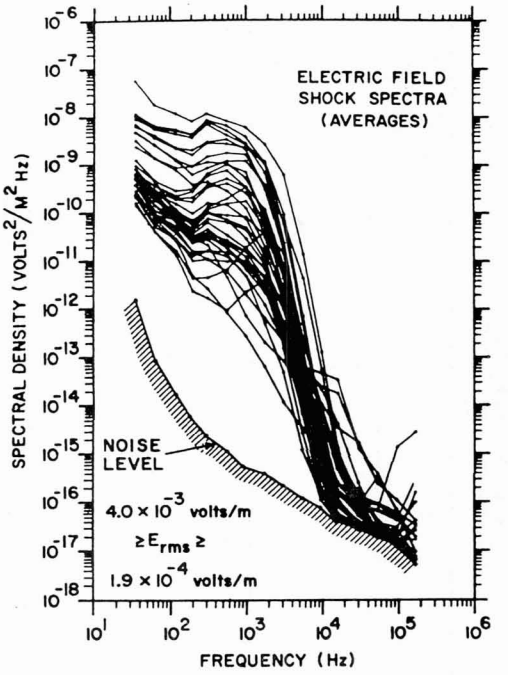

FIG. 22*a*. — The intensity variability of bow shock electric field turbulence is indicated by the representative sample of shock spectra obtained in 36 crossings of the bow shock. The average spectra are 5.13-s averages. E_{rms} is the rms electric field strength obtained by integrating a given spectrum from 20 Hz to 200 kHz [12].

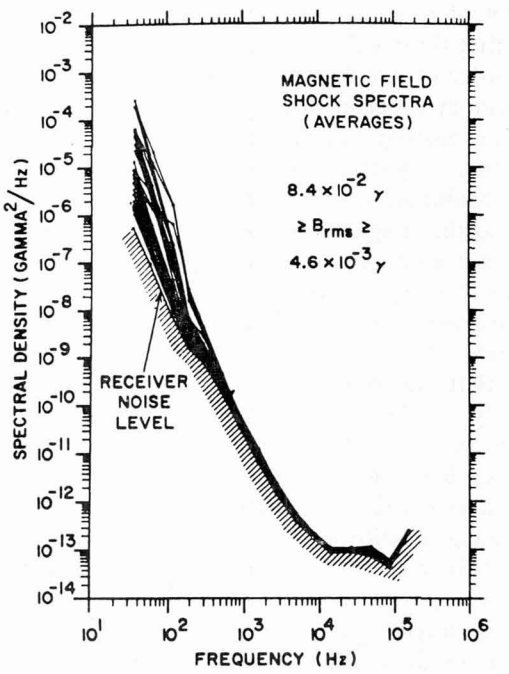

FIG. 22*b*. — The intensity variability of bow shock magnetic field turbulence is represented by average spectra obtained for the same 36 shock crossings shown in figure 22*a*. B_{rms} is the rms magnetic field strength [12].

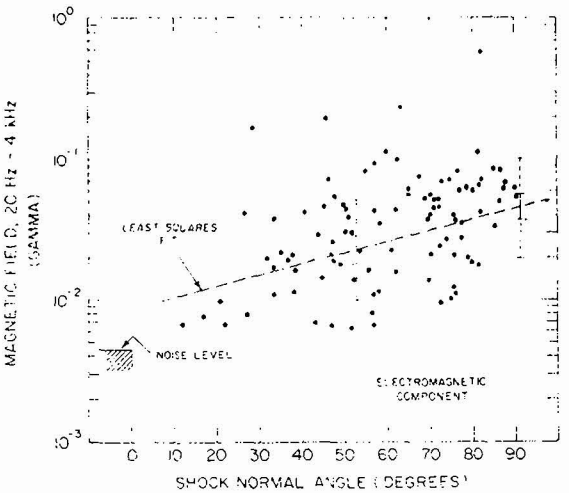

FIG. 23. — Plot of B_{rms} against the shock normal angle $\widehat{Bn}$ showing a positive correlation. The error bars have the same meaning as in figure 5 [12].

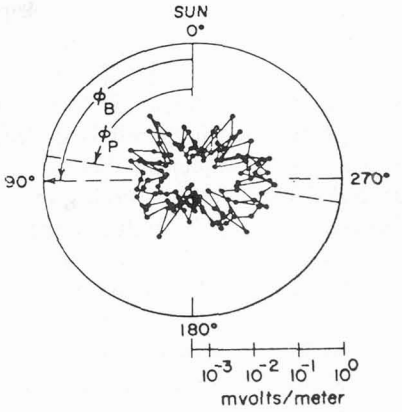

FIG. 24*b*. — The polar plot is a rapid-sample measurement plotted versus the spacecraft spin angle in the solar ecliptic plane and represents the electrostatic turbulence at 31.1 kHz in the leading edge of the shock crossing in figure 24*a*. The orientation of the upstream magnetic field vector is indicated by φ_B. The minor principal axis of the distribution of rapid-sample measurements is indicated by φ_p.

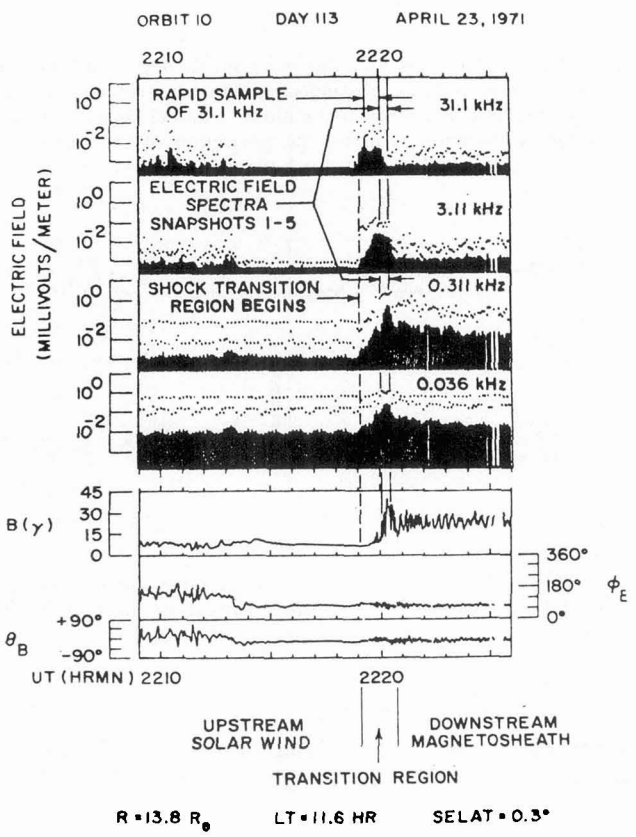

FIG. 24*a*. — A shock crossing which shows the relation between the rise and relaxation times of electric field turbulence at high and low frequencies. Electric field noise is clearly detected ahead of the main gradient in the magnetic field. The solid vertical lines indicate the time intervals for the rapid sample measurement and electric field spectra of figures *b*, *c*. Upstream electrostatic oscillations at 3.11 and 31.1 kHz are correlated with the long-period waves in the magnetic field Shock parameters are $M = 6.9$, $\beta = 1.42$, $T_e/T_p = 1.0$ and $\widehat{Bn} \approx 90°$.

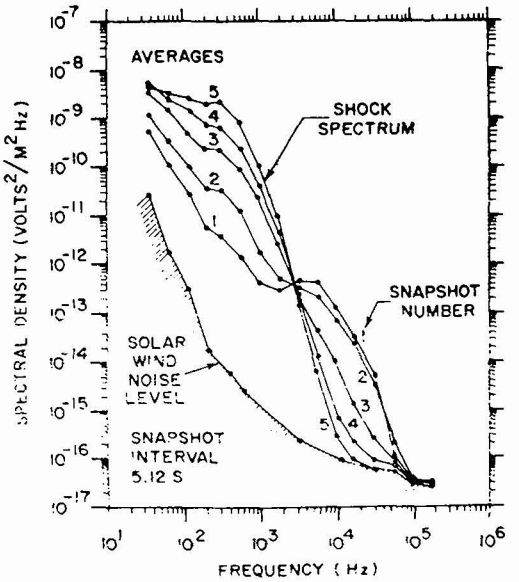

FIG. 24*c*. — The electric field spectra indicate the sequential development of electrostatic turbulence with frequency as the main transition is traversed [12].

noise in four frequency bands is given. During the shock crossing, rapid samples of 31 kHz waves and electric field spectral changes were recorded. In figure 24*b* a polarization study of the 31 kHz noise shows that the polarization axis φ_p is almost along the magnetic field φ_B, the waves, therefore are identified as electron plasma oscillations and are located in the foot of the shock. In figure 24*c* five electric field spectra are shown, taken in the foot (label 1) of the field gradient and through the main magnetic ramp (label 2-5). The broadening of the spectrum of electron plasma oscillations toward lower frequencies indicates the occurrence of electron heating in the leading edge of the shock. As the main ramp is tra-

versed, the electric field spectrum develops a peak at 311 Hz simultaneously with the disappearance of the peak at 3.11 kHz. This peak at 311 Hz (around the ion plasma frequency) corresponds to the occurrence of maximum proton heating, and is developed after electron heating. This sequential behaviour, suggesting a coupling between the two modes, and the observed relationship with T_e/T_i, induces the authors in reference [12] to conclude that their observations are consistent with an electron-proton streaming instability.

When the Mach number increases, the double structure presented above disappears and the shock assumes a broad turbulent structure, see figure 3 in reference [24], although the properties of the turbulence observed within the shock appear to be the same. The wave breaking is revealed mainly in the increase of the amplitude of low frequency magnetic fluctuations.

A comparison of the experimental with theoretical predictions will be avoided here because of the absence of a good, complete theory for $\beta \gtrsim 1$ $M > M^*$ shocks. A review of the suggested old models has been given in reference [4], see also reference [6], and reference [33] where discussions on possible instabilities within the shock layer are given. We certainly feel the need for a good complete theoretical model for these structures.

7. **Quasi electrostatic shocks.** — A shock wave in a collisionless plasma without an external magnetic field ($B_0 = 0$) is necessarily an electrostatic shock, as the sound waves are the only possible oscillations in the medium. A very high beta plasma is a plasma in which the plasma thermal pressure is much higher than the magnetic pressure, i. e. the sound speed is much larger than the Alfvén speed : $C_S \gg C_A$. A priori it is, therefore, reasonable to think that a very high β shock will be electrostatic as in the case of absence of magnetic field. The observations show that this is not completely true, as low frequency electromagnetic waves are observed ; from here the nomenclature of this section.

A few very high β shock observations have been discussed in reference [34] and one of them is reported in figure 25*a*, *b*, *c*. The complete transition from undisturbed solar wind into the downstream plasma, is observed to last as much as 9-10 minutes ! The structure appears to be divided into three regions : the upstream *wave packets* from 0752 to 0758 U. T. (Fig. 25*a*). In this period the average value of B is $1 \div 1.5$ γ and bursts of VLF noise appear regularly, strongly deflecting the solar wind ions. No ion thermalization occurs in this region, while electrons are already heated by the first few packets. Electrostatic noise is observed in this region at 1.3 kHz (around the ion plasma frequency). The *wave packets* appear to be bursts of whistler waves, however they are probably locally generated, as in a high β plasma the

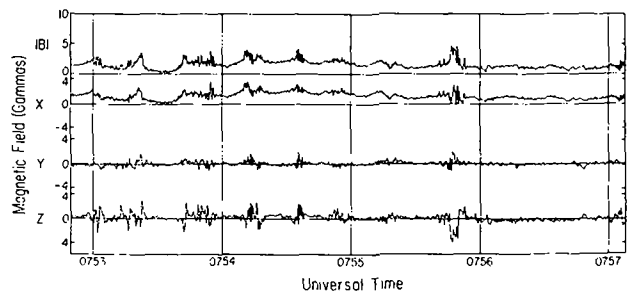

FIG. 25*a*. — *Wave packets* observed upstream at a very high β shock structure with OGO-5 and Day 23, 1969. The field intensity is shown on the top [34].

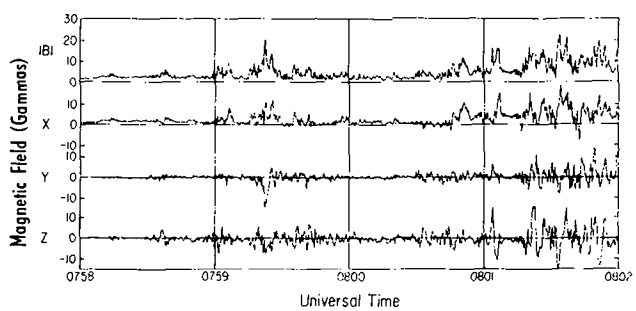

FIG. 25*b*. — The *foot* and the *main gradient* ($\approx$ 0801 U. T.) at the very high β shock crossing-sample rate is seven per second. The Z direction is chosen to be along a model shock normal, and the X direction is along the projection of the upstream field in the shock plane [34].

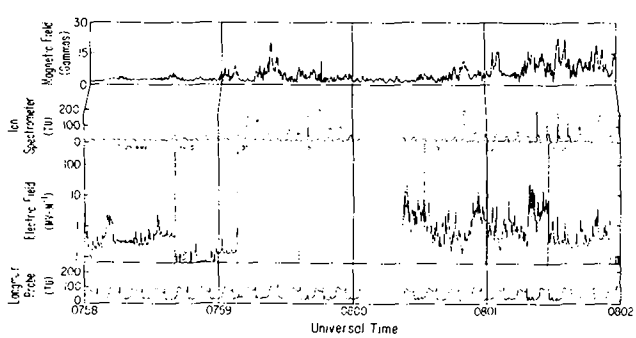

FIG. 25*c*. — Multidiagnostic view of the same shock-crossing. The data are shown in the same format as in figures 15 or 17 [34].

whistler group velocity is not large enough to radiate upstream from a high Mach number shock. From 0758 to 0800 : 30 U. T. a *foot* appears (Fig. 25*b*). This foot is in evidence by the fact that the average field intensity is higher (3-4 γ) and also the bursts of whistler noise appear to be of much larger amplitude. Bursts of electrostatic noise are continuously observed through all this region in the frequency bands of 0.56, 1.3, 3, 7.35 kHz (Fig. 25*c*). The ion thermalization also starts in this *foot* and becomes more intense in coincidence with the bursts of noise. Complete thermalization, however is reached only after the *main ramp* : a larger increase of the average magnetic

field intensity occurring between 0800 : 30 and 0801 : 30 U. T. (Fig. 25*b*). It is interesting to note that in coincidence with the noise bursts the field intensity may become 20-30 times larger than the upstream intensity, and also the ion integral flux may become larger than the upstream value. It is important to note that the magnetic energy in the peaks encountered in the foot and in the shock, were hundreds times larger than the upstream magnetic energy.

In conclusion the wave breaking appears to generate the highly disturbed shock structure. As a consequence this quasi perpendicular structure resembles the quasi parallel structure discussed in the next section. This resemblence is increased by the fact that very low values of Ω_i and Ω_e result in an enlargement of all length scales, in absolute numbers, as it also occurs for quasi parallel shocks [35].

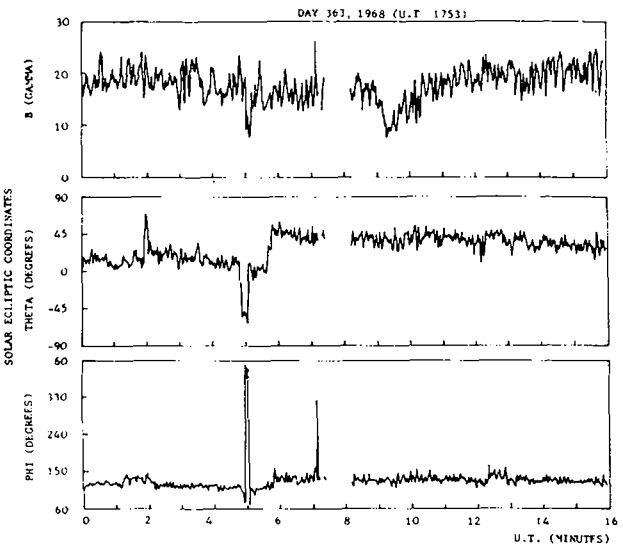

FIG. 26. — Magnetosheath magnetic field intensity B latitude θ and longitude Φ, observed by HEOS-1 downstream at a quasi parallel shock structure on Day 363, 1968 [18].

8. **Quasi parallel structures.** — As mentioned in section 2, for a given magnetic field direction in the solar wind, the earth's bow shock being a three dimensional surface, all values for $\widehat{Bn}$ can be found, therefore the shock will have a quasi perpendicular structure over one half the surface area, and a quasi parallel structure over the other half. 50 % of satellite shock observations should, therefore, show a quasi parallel structure. These structures in space have features not observed in laboratory oblique shock experiments. As we have seen in Section 6 for turbulent shock structures, within the shock layer an accelerating process acts over the ions, generating suprathermal particles. In quasi perpendicular shocks most of the particles try to move along $\bar{B}$ away from the shock, the solar wind carries the line of force in the shock layer, and the suprathermal particles will be seen in the shock moving downstream. If $\bar{B}$ is at a large angle from the shock surface, however (quasi parallel shocks) then the suprathermal particles may actually leave the shock region, and will be found in a vast region upstream of the quasi parallel shock (Fig. 1). The suprathermal particles may then, interact with the incoming plasma and generate instabilities of various kinds. The turbulence thus generated, will then be convected downstream and perhaps amplified through the shock, probably strongly affecting or destroying its structure. It is certain that the low frequency turbulence downstream of quasi parallel structures is higher than in other cases, as it is shown in figure 26 (compare with Figs. 7 and 19). In reference [28] power spectra of shocked magnetic field have been studied for quasi parallel and quasi perpendicular (turbulent) structures : in the first case the power is a factor 10 higher, mainly at low frequencies. In agreement with the theoretical considerations of Tidman and Krall [8] being the quantity in eq. (9) positive and large, the downstream ion energy distribution is of Maxwellian type, as it is shown in figure 9. One of the most important difficulties in studying these structures, is the impossibility of finding the magnetic gradient to be called *the shock*. Indeed in each orbit, when the quasi parallel structure is observed, we may distinguish three very broad regions (each of the order of several earth radii thick). In the first region four different wave phenomena are observed : low frequency magnetosonic waves, plasma waves, whistler wave packets and whistler waves. Figure 27 shows three of these oscillatory phenomena : Figure 27*a* shows a power spectrum with the low frequency peak (0.02 Hz, magnetosonic waves) and with a higher frequency peak (0.55 Hz, whistler wave packets). Figures 27*b*, *c* show low frequency magnetosonic waves together with wave packets or whistler noise, respectively. The magnetosonic waves have been observed only in a region that depends on the magnetic field direction and is geometrically defined by a speed $V_{\parallel} = 2\ V_{S.W.}$ of suprathermal protons flowing backward (see ref. [36]). These low frequency waves are circularly polarized [37], are observed only along lines of force intersecting the shock surface, have an amplitude $10 \div 50$ % of the ambient field and are mainly transverse ; they are attenuated with distance from the bow shock only slightly : a factor 2 in 10-15 R_E. The amplitude of these waves appear to increase with increasing solar wind speed, and decrease with increasing solar wind density [38], in agreement with a theory proposed in reference [39] (see also [40]) in which suprathermal particles travelling upstream interact with the incoming solar wind (two stream instability with ion cyclotron resonance) to generate hydromagnetic wave with the observed polarization amplitude and with the observed attenuation with distance from the shock.

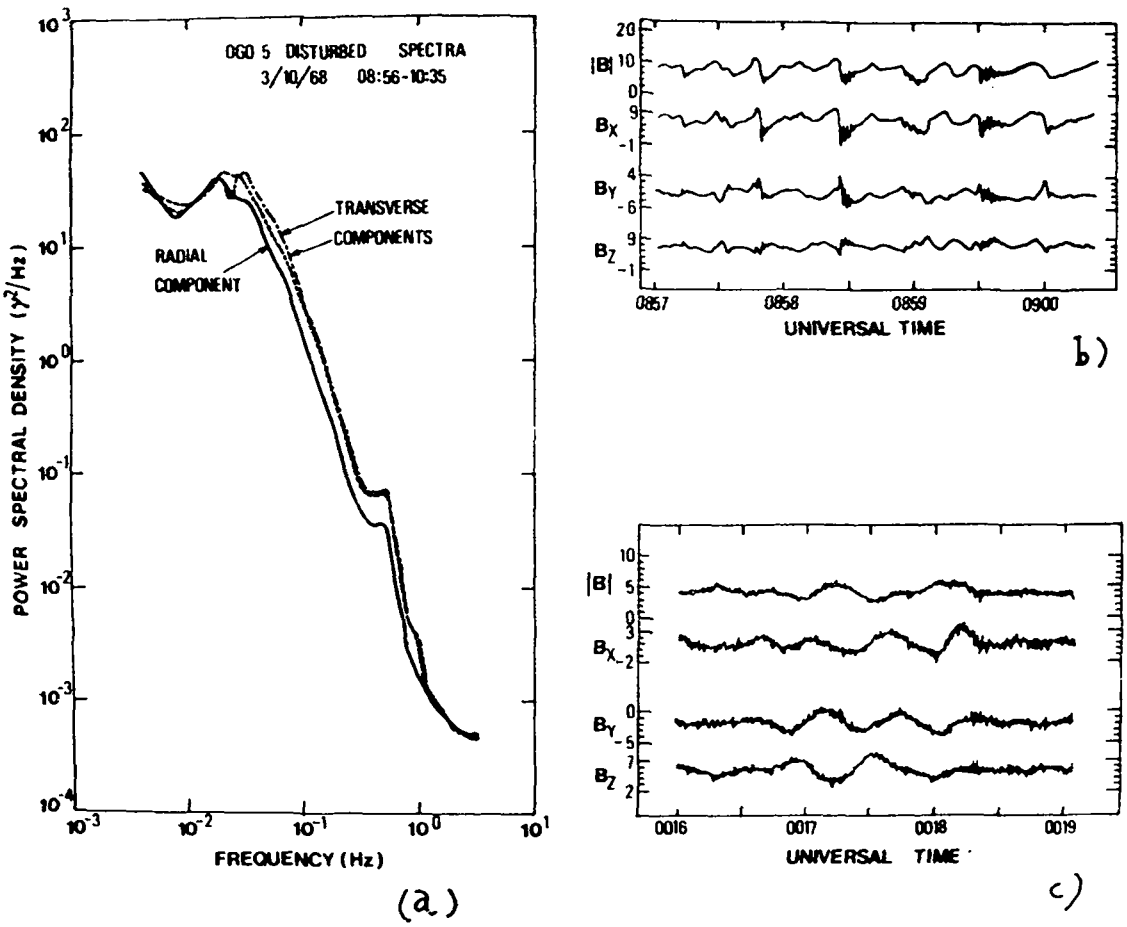

FIG. 27*a*. — OGO-5 power spectrum for the period 0856 to 1035 U. T. March 10, 1968. Spectra are for the radial and transverse components in a heliocentric spherical co-ordinate system : —·—·— transverse components, ——— radial components [41].

FIG. 27*b*. — Discrete wave packets occurring in association with irregular low-frequency waves on March 10, 1968, while the satellite was at 19.1 R_E and at a Sun-Earth-satellite angle of 67.5° [41].

FIG. 27*c*. — Continual high-frequency waves simultaneous with quasi-sinusoidal low-frequency waves on March 8, 1968, while the satellite was at 21.9 R_E and at a Sun-Earth-satellite angle of 61.3° [41].

Together with hydrodynamic waves, whistler wave packets are often observed [41] with a frequency 2-4 times the proton gyrofrequency. These waves are left hand polarized with a group velocity lower than solar wind speed, therefore are locally generated, also several earth radii upstream of the shock. The amplitude envelope of the packets has often a characteristic shape, with a maximum at the trailing edge of the wave packet. A cyclotron wave echo mechanism, discovered in laboratory plasma physics [42] has been suggested [43] for these packets' generation, but it remains to be proved.

Upstream whistler waves ($\simeq$ 1 Hz) have been occasionally observed both in connection with hydromagnetic waves and without them. A systematic investigation of these waves has not been published, as yet ; it appears, however, that the region where they may be observed is not geometrically bound by the $V_{\parallel} = 2\ V_{s.w.}$ relation. Rather, the waves appear along all lines of force intersecting the bow shock, meaning that they are due to particles that may move along the lines of force with a speed

$$V_{\parallel} \gg V_{s.w.} \cdot$$

These whistler waves, therefore, being non-stationary in the shock frame [44] may be due to backstreaming electrons rather than ions, but this has not been demonstrated. Backstreaming electrons have indeed been observed [45, 46, 47, 48, 49] and are causing electron plasma waves in the far upstream region (Fig. 28) [47, 50] probably through stream stream interaction. Also these backstreaming electrons appear to reach regions as far as the moon, where they have been observed.

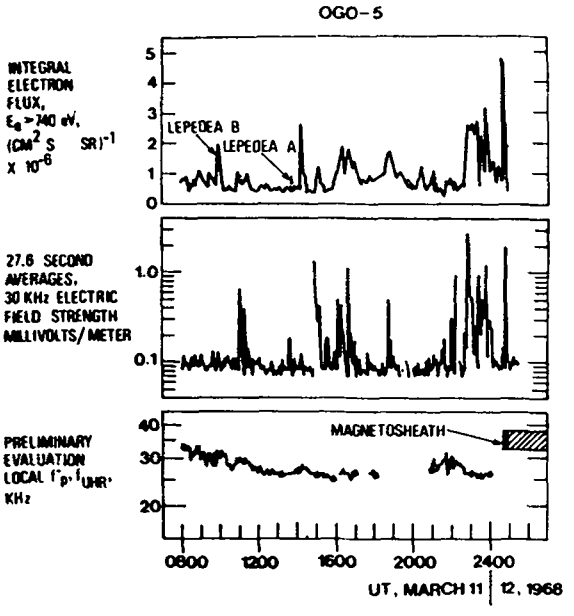

FIG. 28. — Correlation of electrostatic noise and backstreaming electrons upstream of a quasi parallel shock structure : Top panels : comparison of the average 30 kHz field strength and the integral flux of nonthermal electrons. Bottom panel : Local electron plasma and upper hybrid frequencies deduced from the JPL plasma probe data [46].

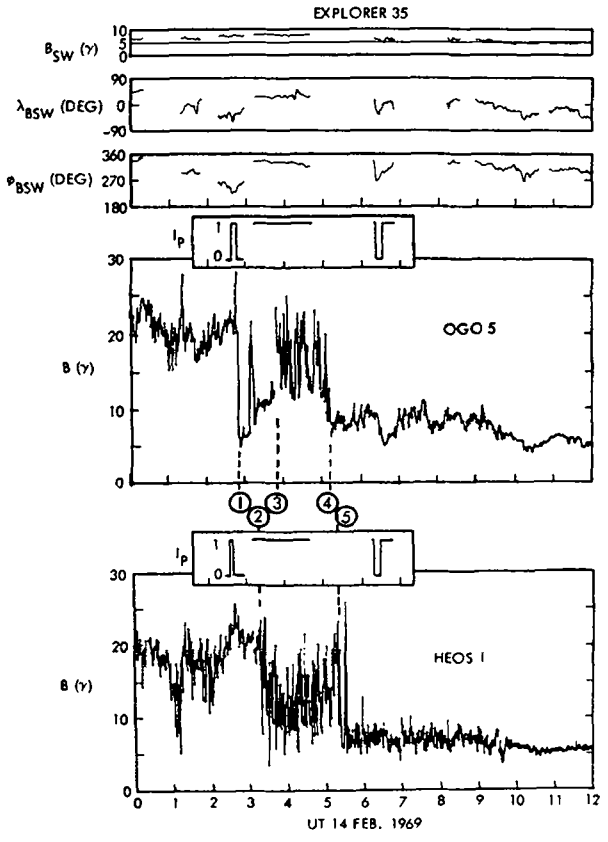

FIG. 29. — Synoptic magnetic field observations of the quasi-parallel bow shock of February 14, 1969. For Explorer 35, 82-s averages are plotted, for OGO-5, 60-s averages ; and for HEOS, 48-s samples. The circled numbers refer to times of boundary crossings or pulsation onsets at either HEOS or OGO [35].

Between the region of the upstream turbulence described above, and the region of downstream plasma state, characterized by the turbulence shown in figure 26 and the Maxwellian ion energy spectrum of figure 9, a third region exists, 2-3 R_E thick, in which the turbulence reaches so high a level that it may be called the *shock*, although many *pulsations* may exist simultaneously in different places, and probably dissipation is occurring simultaneously at those pulsations. These pulsations have been extensively studied in [35] (see also [51*a*, *b*, *c*]) where simultaneous observations by HEOS 1 and OGO-5 of a quasi parallel shock have been published. The value of Mach number and β appear for the moment to be unimportant in the sense that similar, highly turbulent pulsations are observed for different M and β. It should be noted, however, that no quasi parallel laminar shock has been reported in the literature. Magnetic field data for the quasi parallel shock of reference [35] are given in figure 29. Upstream hydromagnetic waves are observed in HEOS-1 between 0515 and $\simeq$ 1 000 U. T. while in OGO-5 they start somewhat earlier. Pulsations are observed between 0315 and 0515 at both satellites. Before 0315 the bow shock, crossed by OGO-5, had a quasi perpendicular structure, as it is indicated by the different interplanetary magnetic field direction. A net change of solar wind plasma properties was observed in the three regions. Figure 30*a* is a graph of three energy distributions from HEOS-1 data superimposed on a common horizontal scale. The ones indicated *solar wind* or *magnetosheath* are averages of several spectra observed after 0520 and before 0315 respectively. The one marked *pulsation region* is the average of all spectra taken during the 2 hours or so of pulsation profile. This spectrum shows the plasma energy peak at, or slightly below, the bulk energy of the solar wind, but with a lower maximum and a broadened, hotter, more skewed ion distribution, as it is confirmed by the two single spectra in figure 30*b*. The fluctuations of particle integral flux and magnetic field intensity appear to be anticorrelated. The pulsations are illustrated in figures 31 and 32 with multidiagnostic data from OGO-5. Figure 31 shows two short bursts of pulsations ; figure 32 shows two data segments out of longer intervals of continuous pulsations. The quasi periodic character of the large oscillations is striking, particularly in the components, as the illustrated B_x shows. The full array of diagnostics demonstrates that the pulsation profiles were neither solar wind nor magnetosheath nor alternating samples of these two regions. The deflection and/or thermalization of the solar wind stream

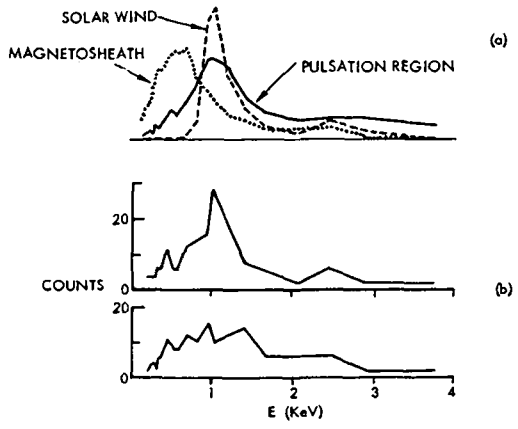

FIG. 30. — Average solar wind, magnetosheath, and pulsation region ion energy spectra from HEOS 1.

FIG. 30*b*. — Two representative pulsation ion spectra [35].

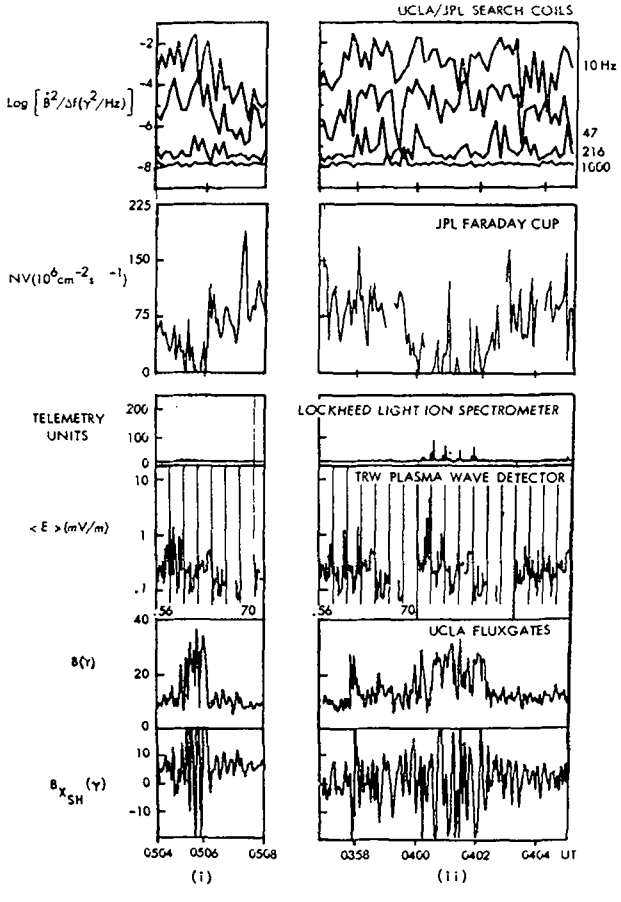

FIG. 31. — Multidiagnostic view of the *pulsating* plasma regime, observed by OGO-5 on February 14, 1969 : Two bursts of pulsations. From the bottom are shown : magnetic field component $B_{X_{SH}}$ along an axis coinciding as close as possible with the projection of $\vec{B}$ in the *shock plane* ; magnetic field intensity B ; electrostatic noise from the T. R. W. plasma wave detector ; Lockheed light ion spectrometer data in telemetry arbitrary units ; J. P. L. Faraday cup integral flux ; and on top the figure electromagnetic noise search coil data observed in the four bands at 10, 47, 216, 1 000 Hz calibrated and plotted on the same vertical scale [35].

was evident in both the J. P. L. and the Lockeed data when the *megapulsations* were present. Electric plasma wave and magnetic E. L. F. wave noise levels were enhanced to values higher than those sustained in the sheath and were comparable to those normally associated with low β low M quasi perpendicular shock crossing. In reference [35] the interpulsation regime has also been discussed : true solar wind data were similar to each other whether representative of unperturbed solar wind, upstream wave onset or *deep* upstream wave observations, while interpulsation waves, appearing to emulate upstream waves magnetically, showed diagnostic features suggestive of a quite different regime. Indeed in the interpulsation regime electromagnetic and electrostatic noise was enhanced in the E. L. F. bands (10 Hz and 0.56-1.3 Hz respectively) and partial thermalization of incoming ions occurred. By means of the two satellite HEOS-1 and OGO-5 data, the thickness of the pulsation region was estimated in reference [35] to be $\lesssim 2\ R_E$. In all this region the solar wind was deflected but not significantly decelerated.

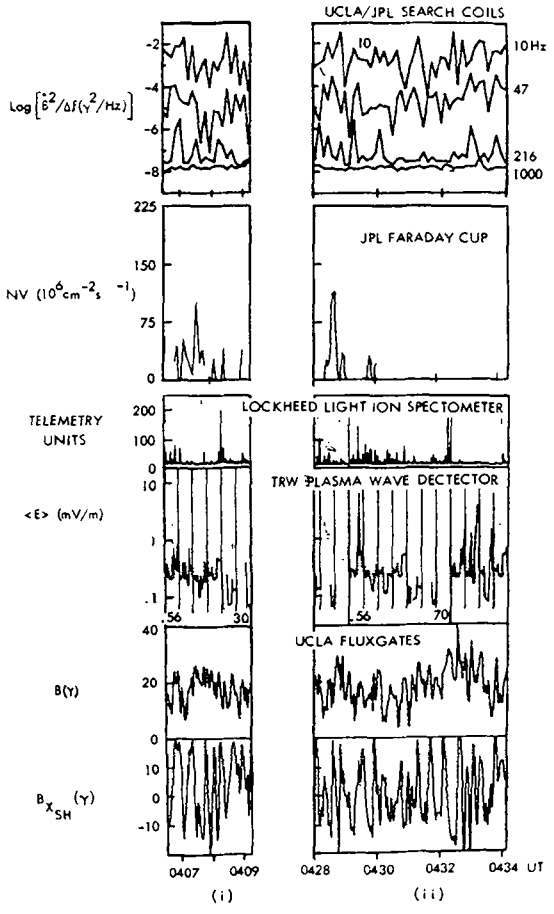

FIG. 32. — Multidiagnostic view of the *pulsating* plasma regime, observed by OGO-5 on February 14, 1969 : continuous pulsations. The data are in the same format as in figure 31 [35].

With reference to the work of Kennel and Sagdeev [52] and Auer and Volk [53], in reference [35] it was shown that no direct evidence was found that the macrostructure was governed by fire hose instability as a dissipation mechanism, rather the macrostructure followed the outlines of an oblique whistler shock, modified by additional irregularity and complexity.

9. **Conclusions.** — In concluding this review we would like to mention the limits of the work done until now and the directions in which work should be done.

We have neglected, in this paper, to review the many published theories for collisionless shock waves, this being outside the scope of our aims. The reader is referred to references [8, 4, 14, 6, 5, 2]. Also the comparison of experimental results with theory, in the high β plasma regimes has been avoided for two reasons : one is that the theories developed on this argument are incomplete because of the many difficulties present [4, 6] they have often a fragmentary aspect. Another reason is, on the contrary, due to incompleteness of the observations : not only did we miss the thickness of the shock structures due to the unknown shock-satellite speed, but also the particle behaviour in the shock layer and their energy spectrum, is still unclear. To avoid theoretical mathematical difficulties computer experiments, only partially used [54] until now, may be further developed.

From an observational point of view we do not know at the moment, if M and β and T_e/T_i are important for the turbulence, or the structure, of the quasi parallel shocks. It is interesting to note, on the other hand, that suprathermal particles generated at the shock and interacting upstream with incoming plasma had not been observed in laboratory experiments, probably due to the small length of the mean free path. Can these upstream features be reproduced and studie in the laboratory ? What are the phenomena causing all the observed waves ?

On another point the theory seems to be ahead of space observations : the mode-mode interaction of the waves, and the decay of the turbulence directely generated in the shock layer into other modes or other frequencies.

In spite of the many difficulties present, we know now that many different theories may be valid in the different regions of the multidimensional phase space concerning collisionless shocks, and our experimental understanding of these interesting phenomena has, in the last years, considerably progressed.

Acknowledgements. — This research was supported by the Consiglio Nazionale delle Ricerche, Italy. The work was completed while holding an ESA fellowship at Space Science Department of ESA, in ESTEC Noordwijk Holland.

References

[1] HUNDHAUSEN, A. J., « Coronal expansion and solar wind », in *Phys. and Chemistry in Space*, 5 (Springer-Verlag, New York), 1972.

[2] PAUL, J. W. M., Review of experimental studies of collisionless shocks propagating perpendicular to a magnetic field, in *Collision-free shocks in the laboratory and Space* (ESRO SP-51), p. 97, 1969.

[3] PAUL, J. W. M., « Collisionless shocks », in *Cosmic Plasma Physics*, ed. by Karl Schindler (Plenum Press), p. 293, 1972.

[4] DOBROWOLNY, M. and FORMISANO, V., « The structure of the earth's bow shock », *Riv. Nuovo Cimento* **3** (1973) 419.

[5] FRIEDMAN, H. W., LINSON, L. M., PATRICK, R. M. and PETSCHEK, H. E., « Collisionless shocks in plasmas ». *Magnetohydrodynamic Annual Review*, 1971.

[6] GALEEV, A. A., « Collisionless shocks », in *Physics of solar planetary environments*, ed. by D. J. Williams, pub. by *Am. Geophys. Union* (Boulder), p. 464, 1976.

[7] SAGDEEV, R. Z., « Cooperative phenomena and shock waves in collisionless plasmas », in *Problemy Teorii Plazmy*, ed. by Leontovich, M. A. (Atomisdat, Moscow), Vol. 4, 1964 and in *Rev. Plasma Physics* ed. by (M. A. Leontovich, New York), p. 23, 1966.

[8] TIDMAN, D. A. and KRALL, N. A., *Shock waves in collisionless plasmas* (Wiley Interscience, ed. N. Y.), 1971.

[9] WOODS, L. C., « Critical Alfvén Mach numbers for transvers field MHD shocks », in *Plasma Phys.* **11** (1969) 25.

[10] WOODS, L. C., « On the structure of collisionless magnetoplasma shock waves at super-critical Alfvén Mach numbers », in *J. Plasma Phys.* **3** (1969) 435.

[11] WHITE, R. B., FRIED, B. D. and CORONITI, F. V., « Structure of ion acoustic solitons and shock waves in a two component plasma ». University of California (UCLA) Internal Note PPG-100, 1971.

[12] RODRIGUEZ, P. and GURNETT, D. A., « Correlation of bow shock plasma wave turbulence with solar wind parameters » in *J. Geophys. Res.* **81** (1976) 2871.

[13] PODGORNY, I. M., ANDRIANOV, Y. V. and DUBININ, E. M., « Electric field microfluctuations on the shock front in the model experiment », in *Astrophys. Space Sci.* **24** (1973) 245.

[14] FORMISANO, V., « The earth's bow shock fine structure », in *Correlated Interplanetary and Magnetospheric Observations* ed. by D. E. Page, D. Reidel Pub. Co. (Dordrecht, Holland), p. 187, 1974.

[15] FORMISANO, V., PALMIOTTO, F. and MORENO, G., « α-particle observations in the solar wind » in *Sol. Phys.* **15** (1970) 479.

[16] GALEEV, A. A., VAISBERG, O. L., ZASTENKER, G. N., ZERZALOV, A. A. and CHOCHLOV, M. Z., in *Fiz. Plasmy* **1** (1975) 441.

[17] FORMISANO, V., HEDGECOCK, P. C., MORENO, G., SEAR, J. and BOLLEA, D., « Observation of the earth's bow shock for low Mach numbers », in *Plan. Space Sci.* **19** (1971) 1915.

[18] FORMISANO, V., HEDGECOCK, P. C., MORENO, G. and PALMIOTTO, F., « Solar wind interaction with the earth's magnetic field. I) The Magnetosheath », in *J. Geophys. Res.* **78** (1973) 3714.

[19] GREENSTADT, E. W., RUSSELL, C. T., SCARF, F. L., FORMISANO, V. and NEUGEBAUER, M., « Structure of the quasi-perpendicular laminar bow shock », in *J. Geophys. Res.* **80** (1975) 502.

[20] FAIRFIELD, D. H. and FELDMAN, W. C., « Standing waves at low Mach number laminar bow shocks », in *J. Geophys. Res.* **80** (1975) 515.

[21] FORMISANO, V. and HEDGECOCK, P. C., « Laminar and quasi-laminar shock structures », in *Nuovo Cimento* **24B** (1974) 1.

[22] FORMISANO, V. and HEDGECOCK, P. C., « Solar wind interaction with the earth's magnetic field. 3) On the earth's bow shock structure », in *J. Geophys. Res.* **78** (1973) 3745.

[23] FORMISANO, V., RUSSELL, C. T., MEANS, J., GREENSTADT E. W., SCARF, F. and NEUGEBAUER, M., « Collisionless shock waves in space. A catalog from the earth's bow shock ». Internal Note, LPS 74-3, 1974.

[24] GREENSTADT, E. W., « Structure of the terrestrial bow shock », in « *Solar Wind Three* », ed. by C. T. Russell (Univ. of California, Los Angeles), p. 440.

[25] ESELEVICH, V. G., EKPOV, A. G., KURTMULLAEV, R. Ch. and MALUTIN, A. I., « Isomagnetic discontinuity in a collisionless shock wave », in *J. Exper. Theor. Fiz.* **60** (1971) 2079.

[26] FORMISANO, V. and KENNEL, C. F., « Small amplitude waves in high β plasmas » in *J. Plasma Phys.* **3** (1969) 55.

[27] NEUGEBAUER, M., RUSSELL, C. T. and OLSON, J. V., « Correlated observations of electrons and magnetic fields at the earth's bow shock », in *J. Geophys. Res.*, **76** (1971) 4366.

[28] AMATA, E., « The calm and turbulent state of the earth's magnetosheath from December 1968 through March 1970 », in *The magnetospheres of the Earth and Jupiter*, ed. by V. Formisano, D. Reidel Publ. Co. (Dordrecht, Holland), p. 25, 1975.

[29] FORMISANO, V. and HEDGECOCK, P. C., « On the turbulent bow shock structure », in *J. Geophys. Res.* **78** (1973) 6522.

[30] MONTGOMERY, M. D., ASBRIDGE, J. R. and BAME, S. J., « Vela 4 plasma measurement observations near the earth's bow shock » in *J. Geophys. Res.* **75** (1970) 1217.

[31] NEUGEBAUER, M., « Initial deceleration of solar wind positive ions in the earth's bow shock », in *J. Geophys. Res.* **75** (1970) 717.

[32] RODRIGUEZ, P. and GURNETT, D. A., « Electrostatic and electromagnetic turbulence associated with the earth's bow shock », in *J. Geophys. Res.* **80** (1975) 19.

[33] GREENSTADT, E. W. and FREDRICKS, R. W., « Plasma instability modes related to the earth's bow shock », in *Magnetospheric Physics*, ed. by B. M. McCormac, D. Reidel (Publ. Co., Dordrecht, Holland), p. 281, 1974.

[34] FORMISANO, V., RUSSELL, C. T., MEANS, J. D., GREENSTADT, E. W., SCARF, F. L. and NEUGEBAUER, M., « Collisionless shock waves in space : A very high β structure », in *J. Geophys. Res.* **80** (1975) 2013.

[35] GREENSTADT, E. W., RUSSELL, C. T., FORMISANO, V., HEDGECOCK, P. C., SCARF, F. L., NEUGEBAUER, M. and HOLZER, R. E., « Structure of a quasi-parallel, quasi-laminar bow shock », in *J. Geophys. Res.* **82** (1977) 651.

[36] DIODATO, L., GREENSTADT, E. W., MORENO, G. and FORMISANO, V., « A statistical study of the upstream wave boundary outside the earth's bow shock », in *J. Geophys. Res.* **81** (1976) 199.

[37] FAIRFIELD, D. J., « Bow shock associated waves observed in the far upstream interplanetary medium », in *J. Geophys. Res.* **74** (1969) 3541.

[38] FORMISANO, V. and AMATA, E., « Solar wind interaction with the earth's magnetic field. 4) Preshock perturbation of the solar wind », in *J. Geophys. Res.* **81** (1976) 3907.

[39] BARNES, A., « Theory of bow shock associated hydromagnetic waves in the upstream interplanetary medium », in *Cosmic Electrodynamics* **1** (1970) 90.

[40] FREDRICKS, R. W., « A model for generation of bow shock associated upstream waves », in *J. Geophys. Res.* **80** (1975) 7.

[41] RUSSELL, C. T., CHILDERS, D. D. and COLEMAN, P. J., « OGO-5 observations of upstream waves in the interplanetary medium : discrete wave packets », in *J. Geophys. Res.* **76** (1971) 845.

[42] FRIED, B. D. and OLSON, C., « Transverse plasma wave echoes » in *Phys. Rev.* **180** (1969) 241.

[43] WU, C. S., « Theory of discrete wave packets in the solar wind », in *J. Geophys. Res.* **77** (1972) 575.

[44] HOLTZER, R. E., OLSON, J. V., RUSSELL, C. T. and NORTHROP, T. G., « A study of waves in the earth's bow shock », in *J. Geophys. Res.* **77** (1972) 2264.

[45] ANDERSON, K. A., « Energetic electrons of terrestrial origin upstream in the solar wind », in *J. Geophys. Res.* **73** (1968) 2387

[46] FREDRICKS, R. W., SCARF, F. L. and FRANK, L. A., « Nonthermal electrons and high frequency waves in the upstream solar wind : 2) Analysis and interpretation », in *J. Geophys. Res.* **76** (1971) 6691.

[47] SCARF, F. L., FREDRICKS, R. W., FRANK, L. A., RUSSELL, C. T., COLEMAN, P. J. and NEUGEBAUER, M., « Direct correlations of large amplitude waves with superthermal protons in the upstream solar wind », in *J. Geophys. Res.* **75** (1970) 7316.

[48] SCARF, F. L., FREDRICKS, R. W., FRANK, L. A. and NEUGEBAUER, M., « Nonthermal electrons and high frequency waves in the upstream solar wind : 1) observations », in *J. Geophys. Res.* **76** (1971) 5162.

[49] REASONER, D. L., « Observations of low energy electrons upstream of the earth's bow shock », in *J. Geophys. Res.* **80** (1975) 187.

[50] FREDRICKS, R. W., SCARF, F. L. and GREEN, I. M., « Distribution of electron plasma oscillations upstream from the earth's bow shock », in *J. Geophys. Res.* **77** (1972) 1300.

[51] GREENSTADT, E. W., GREEN, I. M., INOUYE, G. T., COLBURN, D. S., BINSACK, J. H. and LYON, E. F., « Dual satellite observations of the earth's bow shock : I) The thick pulsation shock », in *Cosmic Electrodynamics*, **1**, 160, 1970. II) Field aligned upstream waves, in *Cosmic Electrodynamics*, **1**, 279, 1970. « III) Field determined shock structure », in *Cosmic Electrodynamics* **1** (1970) 316.

[52] KENNEL, C. F. and SAGDEEV, R. Z., « Collisionless shock waves in high β plasmas-II », in *J. Geophys. Res.* **72** (1967) 3303.

[53] AUER, R. D. and VÖLK, H. J., « Parallel high β shocks and relaxation phenomena » in *Astrophys. and Space Sci.* **22** (1973) 243.

[54] PAPADOPOULOS, K., « Ion thermalization in the earth's bow shock », in *J. Geophys. Res.* **76** (1971) 3806.